Carbon export and transfer to depth across the Southern Ocean Great Calcite Belt

S. Z. Rosengard[1,2], P. J. Lam[1,3], W. M. Balch[4], M.E. Auro[1], S. Pike[1], D. Drapeau[4], and B. Bowler[4]

[1] Woods Hole Oceanographic Institution, Woods Hole, MA
[2] Massachusetts Institute of Technology, Cambridge, MA
[3] University of California, Santa Cruz, CA
[4] Bigelow Laboratory for Ocean Sciences, Boothbay Harbor, ME

Correspondence to: srosengard@whoi.edu, pjlam@ucsc.edu

Abstract

Sequestration of carbon by the marine biological pump depends on the processes that alter, remineralize and preserve particulate organic carbon (POC) during transit to the deep ocean. Here, we present data collected from the Great Calcite Belt, a calcite-rich band across the Southern Ocean surface, to compare the transformation of POC in the euphotic and mesopelagic zones of the water column. The ^{234}Th-derived export fluxes and size-fractionated concentrations of POC, particulate inorganic carbon (PIC), and biogenic silica (BSi) were measured from the upper 1000 m of 27 stations across the Atlantic and Indian sectors of the Great Calcite Belt. POC export out of the euphotic zone was correlated with BSi export. PIC export was not, but did correlate positively with POC flux transfer efficiency. Moreover, regions of high BSi concentrations, which corresponded to regions with proportionally larger particles, exhibited higher attenuation of >51 μm POC concentrations in the mesopelagic zone. The interplay among POC size partitioning, mineral composition and POC attenuation suggests a more fundamental driver of POC transfer through both depth regimes in the Great Calcite Belt. In particular, we argue that diatom-rich communities produce large and labile POC aggregates, which generate high export fluxes but also drive more remineralization in the mesopelagic zone. We observe the opposite in communities with smaller calcifying phytoplankton, such as coccolithophores. We hypothesize that these differences are influenced by inherent differences in the lability of POC exported by different phytoplankton communities.

1 Introduction

The biological pump sequesters atmospheric carbon dioxide (CO_2) in the ocean (Volk and Hoffert, 1985) by way of phytoplankton-driven CO_2 fixation, followed by the sinking of this fixed particulate organic carbon (POC) as aggregates and fecal pellets down the water column (Riley et al., 2012). The quantity per unit area and time of POC exiting the base of the euphotic zone defines the export flux, while export efficiency represents the fraction of bulk primary production comprising this flux (Buesseler, 1998). In the mesopelagic zone (from the base of the euphotic zone to ~1000 m), export flux attenuates due to remineralization mediated by zooplankton grazing and bacteria (Buesseler and Boyd, 2009; Giering et al., 2014; Martin et al., 1987). The flux of this processed organic carbon leaving the mesopelagic zone, only ≤10% of export flux, directly scales with the quantity of atmospheric CO_2 sequestered by the marine biological pump over hundreds to thousands of years (Kwon et al., 2009).

On average, only ~1% of the organic matter produced by phytoplankton in the surface reaches the deep sea (Martin et al., 1987). However, export and sequestration flux vary widely by region, as do export efficiencies and attenuation of export flux (Buesseler and Boyd, 2009; Buesseler et al., 2007; Henson et al., 2012b; Henson et al., 2011; Martin et al., 1987; Thomalla et al., 2008). Such variations may drive observed differences in the weight percent of organic carbon deposited at the sediment surface (Hedges and Oades, 1997), suggesting that the overall strength of the biological pump as a carbon sink is not globally uniform. These geographical differences have spurred decades of research into how mechanisms in the shallower ocean – the euphotic and mesopelagic zones – alter sinking particulate organic matter during vertical transit.

As an example, Armstrong et al. (2002), Klaas and Archer (2002) and Francois et al. (2002) posited that mineral associations with sinking organic carbon could explain these variations. Their ballast hypothesis model suggested that minerals enhanced the biological pump (1) by increasing the density, and consequently, the sinking speed of particulate organic matter and (2) by inhibiting organic carbon remineralization down the water column. Expediting vertical transit decreases the time for remineralization to act on sinking particulate organic matter, increasing its chances of reaching the deep sea. The

authors observed that calcite flux in the bathypelagic zone (>1000 m) explains roughly half of the variation in the magnitude of POC flux reaching the deep sea (Klaas and Archer, 2002), and may also account for some of the observed geographical variation in POC flux attenuation with depth (Francois et al., 2002).

In its conception and infancy, the ballast hypothesis was based upon observed correlations between mineral and organic carbon fluxes in the deep (>1000 m) sea. Yet, evidence for the ballast mechanism in the euphotic and mesopelagic zones remains equivocal, as deeper correlations are scarcely matched by shallower ocean observations (Le Moigne et al., 2012). Several surface regions do not exhibit ballast correlations between mineral flux and POC flux (e.g., Thomalla et al., 2008; Henson et al., 2012b). In the Atlantic and Southern Oceans, Le Moigne et al. (2012) found a significant fraction of POC export flux to remain unassociated with minerals altogether. Moreover, tank incubations simulating POC and mineral suspensions yield conflicting results: some have observed mineral associations to increase aggregate sinking rates (Engel et al., 2009), while others find no such effect (Passow and De la Rocha, 2006). De La Rocha et al. (2008) even suggest that sticky polymers from POC might ballast sinking minerals, rather than vice-versa.

The scarcity of evidence supporting a shallow ocean ballast mechanism suggests that the transit of particulate organic carbon in the surface, mesopelagic and deeper ocean is mechanistically de-coupled (Lam et al., 2011; Lomas et al., 2010). Indeed, the debate surrounding the ballast hypothesis arises from a deeper issue of whether the mechanisms that influence carbon export from the euphotic zone are the same as those that control its remineralization in the mesopelagic zone, and/or its transfer beyond the mesopelagic zone into the deep sea.

The following report compares the export of organic carbon from the euphotic zone with its transfer through the mesopelagic zone across the region of the Great Calcite Belt (Balch et al., 2011a; Balch et al., 2014; Fig. 1). Spanning across the Southern Ocean, particularly between the Subtropical and Polar Fronts, the Great Calcite Belt defines a highly reflective band observed from space during each austral spring and summer. Its high reflectivity is caused by calcite-rich surface waters produced by coccolithophore blooms in the Southern Ocean. In this zone, coccolithophores are more abundant than in

regions north and south of the Belt. South of the Polar Front, coccolithophore abundances decline dramatically as dissolved silica concentrations increase and diatoms flourish (Balch et al., 2011a).

Spanning a large range in surface mineral concentrations, primary productivity, and phytoplankton community composition (Balch et al., 2011a), the Great Calcite Belt provides an excellent opportunity to assess the processes controlling organic carbon export, export efficiency, and attenuation of POC concentration ([POC]) with depth. Here, we report estimates of ^{234}Th-derived POC fluxes and [POC] through both the euphotic and mesopelagic zones within the Atlantic and Indian sectors of the Great Calcite Belt. We focus on the upper 1000 m of the Great Calcite Belt because the attenuation of POC flux and concentration is most dramatic within this depth interval (Martin et al., 1987; Lam et al., 2011). As the following discussion illuminates, this study additionally weighs the ballast hypothesis against other mechanisms hypothesized to control the transfer of organic carbon through the water column, and ultimately into the deep sea, where carbon residence time modulates atmospheric pCO_2 and climate over hundreds to thousands of years (Kwon et al., 2009).

2 Methods

2.1 Field site

Samples from the Great Calcite Belt were collected during two research cruises, GB1 and GB2, which transited the Atlantic and Indian sectors of the Great Calcite Belt during the austral summer of 2011 and 2012, respectively (Fig. 1), concurrent with the putative coccolithophore bloom (Balch et al., 2011a). In 2011, for cruise GB1 (MV1101), the *R/V Melville* crossed the Atlantic sector from Punta Arenas, Chile to Cape Town, South Africa, sampling between 39°S and 59°S. One year later, for cruise GB2 (RR1202), the *R/V Revelle* crossed the Indian sector from Durban, South Africa to Perth, Australia, sampling between 37°S and 60°S (Table 1). Both cruise tracks crossed the Subtropical, Subantarctic and Polar fronts, which are approximately located at 40°S, 45°S

and 52°S (e.g., Belkin and Gordon, 1996; Sokolov and Rintoul, 2009), respectively, defining observed shifts in temperature and nutrient characteristics of the surface ocean.

Each day during GB1 and GB2, 30-L Niskin samples were collected pre-dawn for measuring primary production. A Biospherical Instruments (San Diego, CA) sensor was mounted on the CTD/rosette and referenced to a deck sensor mounted on the ship's superstructure to measure Photosynthetically Available Radiation (PAR) during the casts. Water was then sampled at fixed light depths relative to surface irradiance to match light levels in deck-board incubators: 36.5%, 21.1%, 11.7%, 3.55%, 1.93% and 0.28%. The light depths were calculated two ways: (a) between 10:00 and 14:00 h local time (during daylight hours), percentages of surface irradiance were derived directly from the downcast PAR profile immediately preceding bottle firing, or (b) at all other times, the light levels were back-calculated from the previously-determined relationship between beam transmittance and diffuse attenuation of PAR (Balch et al., 2011b). From these casts, primary production rates were measured using the ^{14}C microdiffusion technique (Paasche and Brubak, 1994) with modifications by Balch et al. (2000) (see also (Fabry and Balch, 2010).

2.2 Size-fractionated particle collection

We report measurements of total and particulate ^{234}Th activity and size-fractionated particle composition from 27 stations (Fig. 1; Table 1).

Size-fractionated particles were collected at eight depths in the upper 1000 m of fourteen stations from GB1 and thirteen stations from GB2, using modified battery operated in-situ pumps (McLane WTS-LV). The modified pumps directed seawater through two flow paths (Lam et al., 2014), each of which passed through a "mini-MULVFS" filter holder designed to retain large particles (Bishop et al., 2012). Seawater first passed through 51 μm polyester pre-filters in both filter holders for collection of large (>51 μm) size-fraction particles, and then through paired 0.8 μm polyethersulfone (Supor™) filters in one flow path and paired 1 μm quartz fiber (Whatman™ QMA) filters in the other flow path, both of which collected small (<51 μm) size-fraction particles. An average of 200 L and 500 L of seawater passed through the Supor and QMA

flow paths over 1-2.5 hours, respectively. Immediately after collection, half to all of the >51 μm size-fraction particles from one flow path were rinsed off of the polyester pre-filters and onto 25 mm 1 μm Sterlitech silver filters using 0.2 μm-filtered seawater, and dried at 50°C for subsequent analysis of particulate ^{234}Th, particulate organic carbon (POC), and particulate inorganic carbon (PIC, or calcium carbonate). Subsamples of QMA filters were likewise dried at 50°C for ^{234}Th and POC analysis in the <51 μm size-fraction. Finally, the polyester pre-filters from the other flow path and Supor filters were dried in a laminar flow hood at room temperature.

In the euphotic zone, where most POC is produced, these operationally defined size fractions allude primarily to the structure of phytoplankton communities producing POC (e.g., large diatoms would be found in >51 μm size-fraction particles). In the mesopelagic zone, which extends from the base of the euphotic zone to 1000 m in depth, >51 μm POC is predominantly comprised of phytoplankton and bacterial biomass that has been repackaged into aggregates and fecal pellets. The >51 μm particles collected at station GB1- 85 illustrate these different size-fraction interpretations by depth. Shallower particles collected at 25 m and 73 m, the base of the euphotic zone, are mainly comprised of intact phytoplankton cells (Figs. 2a, 2b). By contrast, deeper particles collected at 173 m exhibit the features of particulate aggregates and fecal pellets (Fig. 2c).

2.3 Particle composition

Bulk concentrations of POC, PIC, biogenic silica (BSi), and particulate ^{234}Th activity were measured in both <51 μm and >51 μm fractions of particles collected at each station. POC concentrations were measured at all depths of the profiles, while [PIC] and [BSi] were mainly measured at select depths above 200 m and at the deepest depth (800-1000 m) of the profile. Particulate ^{234}Th activities in all sub-fractions of >51 μm (25 mm silver filters) and <51 μm (25 mm QMA filters) samples were measured using low level Risø beta counters immediately on the ship and in the lab at least six ^{234}Th half-lives post-collection for background activity.

After counting for ^{234}Th background activity, ~25% of the silver filter (~ 115 L equivalent) was fumed overnight (12-17 hours) with concentrated hydrochloric acid to

192 remove inorganic carbon, before measuring >51 μm [POC] using an elemental CHN
193 analyzer. A similar protocol was followed to measure <51 μm [POC] from one 12 mm-
194 diameter subsample of each QMA filter, representing ~1% of the entire sample (~5 L
195 equivalent). Vertical profiles of >51 μm and <51 μm [POC] between the base of the
196 euphotic zone and the deepest measurement at 800 – 1000 m were fitted to a power-law
197 function to describe the attenuation of [POC] with depth, based on a function first applied
198 to POC flux by Martin et al. (1987) and then analogously to POC concentration by Lam
199 and Bishop (2007),

200 $$[\mathrm{POC}]_z = [\mathrm{POC}]_0 \left(\frac{z}{z_{PAR}}\right)^{-b} \quad (1)$$

201 where, at most stations, z_{PAR} represents the depth of 0.3% photosynthetically available
202 radiation (see Sect. 2.4). The exponent b represents the attenuation coefficient, with
203 higher attenuation coefficients (more negative exponents) for profiles with greater
204 attenuation of >51 μm [POC] with depth. We focus our discussion on the attenuation of
205 >51 μm [POC], because we assume that they contribute disproportionately to sinking
206 fluxes compared to the <51 μm size fraction (McCave, 1975; Lam and Bishop, 2007;
207 Lam et al., 2011). Figure 3 and Table 2 show all significant ($p<0.05$) power law fits for
208 >51 μm [POC] profiles.
209 PIC in the samples was assumed to be biomineral calcium carbonate ($CaCO_3$),
210 and was derived from particulate calcium (Ca) corrected for salt Ca using a seawater
211 0.0382 Ca:Na (g:g) ratio (Lam and Bishop, 2007; Pilson, 2012). In the in-situ pump
212 samples, salt-derived Ca typically accounted for ~60% of total Ca. The >51 μm PIC size-
213 fraction concentrations were measured mainly in subsamples of remaining pre-filter
214 material and occasionally in sub-fractions of the silver filters, if the former were
215 unavailable. The <51 μm size fraction [PIC] was measured in three 12mm circular QMA
216 subsamples, representing ~15 L or ~3% of the sample. Subsamples were leached in 0.6 N
217 ultrapure Sea-Star™ Baseline hydrochloric acid (HCl) at 60°C for 12-16 hours. The
218 leachate was subsequently filtered through a 0.4 μm polycarbonate membrane filter,
219 diluted to 0.12 N HCl, and spiked with 1 ppb of Indium as an internal standard. The
220 spiked leachate solution was then analyzed for Ca, Na and P using an Element 2 sector-
221 field inductively-coupled plasma mass spectrometer (ICP-MS) in medium and high

resolution. Counts per second were converted to concentration using external mixed element standard curves.

For measuring >51 μm and <51 μm [BSi], prefilter or Supor subsamples, respectively, were leached in 0.2 N sodium hydroxide at 85°C for one hour, and analyzed by standard spectrophotometric detection of the blue silico-molybdate complex in each leachate within 24 hours of the leach (Strickland and Parsons, 1968; Brzezinski and Nelson, 1989). Absorbance through each sample was converted to concentration using an external Si standard curve.

2.4 ^{234}Th-derived flux estimates

Particle fluxes were estimated at each station by measuring the water-column disequilibrium between ^{234}Th and ^{238}U in the upper 350 m of the water-column (Savoye et al., 2006). ^{234}Th is the radioactive daughter of ^{238}U with a short enough half-life (24.1 days) relative to ^{238}U such that it is assumed to be in secular equilibrium with its parent isotope in the absence of particle scavenging (i.e., ^{234}Th activity = ^{238}U activity). Disequilibria between the two isotope activities in the water column are attributed to the scavenging of ^{234}Th by sinking particles (Savoye et al., 2006). Integrating the deficit in ^{234}Th relative to ^{238}U provides a measure of particle flux down the water column (Buesseler et al., 2006). Because of the short half-life of ^{234}Th, deviation from secular equilibrium exists only in regions of high particle flux. Thus, ^{234}Th-based flux estimates are most frequently applied in the euphotic zone of the ocean where particle export is maximal.

^{234}Th-^{238}U deficits were determined by measuring total water-column activities of both isotopes. ^{238}U activity ($A_{U\text{-}238}$) profiles were calculated from salinity by the following relationship (Owens et al., 2011):

$$A_{\mathrm{U-238}}\left(\frac{\mathrm{dpm}}{\mathrm{L}}\right) = (0.0786 \times \mathrm{Salinity}) - 0.315 \qquad (2)$$

Total water-column ^{234}Th activity ($A_{Th\text{-}234}$) profiles were determined from 4 L seawater samples collected by CTD casts down to 300-350 m at each station (Pike et al., 2005). Shortly after collection, each 4 L seawater sample was acidified to pH 2 using concentrated nitric acid (HNO_3), spiked with 1 g of ^{230}Th of a known activity (50.06 dpm

g^{-1}) as a yield monitor, equilibrated for 8 hours, and finally brought up to pH 8.5 using ammonium hydroxide (NH_4OH) (van der Loeff et al., 2006). Manganese chloride ($MnCl_2$) and potassium permanganate ($KMnO_4$) were added to the neutralized seawater to form a manganese oxide (MnO_2) precipitate, which efficiently scavenges both natural ^{234}Th and added ^{230}Th. After 12 hours, the precipitate was filtered onto a quartz fiber filter, dried at 50°C, and then mounted beneath a sheet of Mylar and aluminum foil. ^{234}Th activity in the precipitate was measured on board by low level Risø beta counters and post-cruise after at least six ^{234}Th half-lives for background activity. The ^{230}Th spike was recovered by fully dissolving the MnO_2 precipitate, adding a 1 g spike of ^{229}Th of a known activity (69.74 dpm g^{-1}), and measuring ^{229}Th:^{230}Th ratios on an Element 2 sector-field ICP-MS in low resolution. Recovery of ^{230}Th spike was derived from this ratio, and used to correct for inefficiencies in the scavenging of total seawater ^{234}Th by MnO_2 precipitation.

To calibrate beta counting efficiency for each cruise, total deep water (i.e., below 2000 m) ^{234}Th activities were compared to total deep water ^{238}U activities, as measured in 4-5 replicate samples from 2-3 deep water CTD casts during each cruise (at 5000 m during GB1, and at 2500 m during GB2). Beta counting efficiencies were adjusted such that ^{234}Th and ^{238}U activities were equal in these deep measurements, as secular equilibrium would be expected at such depths. We only report upper water-column activities (<350 m) after correcting for experimental efficiencies in both the seawater collection process and beta detector counting. Uncertainties in the total ^{234}Th activity profiles averaged 4.5% and were propagated from errors associated with counting statistics, recoveries, and beta-counting efficiency.

To calculate ^{234}Th export flux, ^{234}Th activity deficits were integrated down to the base of the euphotic zone (z_{PAR}) (Buesseler et al., 2008; Thomalla et al., 2008):

$$^{234}\text{Th Flux}\left(\frac{\text{dpm}}{\text{m}^2\text{d}}\right) = \int_0^{z_{PAR}} (A_{\text{U}-238} - A_{\text{Th}-234})\, dz \qquad (3)$$

At most stations, the export depth, z_{PAR}, was chosen to be the depth where light levels were 0.3% of surface-level PAR. The exception was station GB2-27, which did not include a PAR measurement profile. For this station, the z_{PAR} value of 105 m was defined as the depth where the transmissometry-based particle concentration decreased. These export depths were compared to one additional metric describing particle concentration in

seawater: the depths where ^{234}Th and ^{238}U activities re-established secular equilibrium, or $z_{Th/U}$. We explore the sensitivity of ^{234}Th flux estimates to choice of z_{PAR} in Sects. 3 and 4.1.

^{234}Th flux estimates were converted to POC, PIC and BSi fluxes by multiplication with ratios of >51 μm POC, PIC, and BSi concentrations to particulate ^{234}Th activity in samples at z_{PAR} (Thomalla et al., 2008; Sanders et al., 2010):

$$\text{POC Flux}\left(\frac{\text{umol}}{\text{m}^2\text{d}}\right) = [\text{POC}]: A_{\text{Th}-234} \times {}^{234}\text{Th Flux}\left(\frac{\text{dpm}}{\text{m}^2\text{d}}\right) \quad (4)$$

$$\text{PIC Flux}\left(\frac{\text{umol}}{\text{m}^2\text{d}}\right) = [\text{PIC}]: A_{\text{Th}-234} \times {}^{234}\text{Th Flux}\left(\frac{\text{dpm}}{\text{m}^2\text{d}}\right) \quad (5)$$

$$\text{Si Flux}\left(\frac{\text{umol}}{\text{m}^2\text{d}}\right) = [\text{BSi}]: A_{\text{Th}-234} \times {}^{234}\text{Th Flux}\left(\frac{\text{dpm}}{\text{m}^2\text{d}}\right) \quad (6)$$

2.5 Interpolation of data

In all cases where ^{234}Th activity, >51 μm and <51 μm [POC] and mineral concentrations, and >51 μm particulate ^{234}Th measurements were unavailable at z_{PAR}, linear interpolations between the sampling depths above and below z_{PAR} were used to estimate a value at the export depth (Table 1). The >51 μm and <51 μm size-fraction POC concentrations were interpolated by the power law attenuation function when fits were significant ($p<0.05$), or linearly when these power-law fits were not significant or inconsistent with the broader shape of the [POC] profile at that particular station. In general, corresponding POC:^{234}Th, BSi:^{234}Th, and PIC:^{234}Th ratios are quotients of these interpolated values except as noted in Tables 2 and 3.

3 Results

^{234}Th activity profiles were measured over the upper 300 – 350 m at the 27 stations of cruises GB1 and GB2 (Fig. 4; Table S1). Each activity profile is associated with two metrics that have been used in previous studies to define the export depth (see Sect. 2.4): the base of the euphotic zone (z_{PAR}), which we define at 0.3% surface photosynthetically available radiation (PAR) (e.g., Buesseler and Boyd 2009), and $z_{Th/U}$, where ^{234}Th and ^{238}U activities re-establish secular equilibrium (Table 1). In most

stations, profiles exhibited ^{234}Th activity deficits over a range from surface to 75 – 170 m in depth, below which ^{234}Th activity generally returned to secular equilibrium with ^{238}U activity, within error. The notable exceptions were profiles at stations GB1-6, and GB1-16, which did not return to secular equilibrium by 170 m in depth. Considering that stations GB1-6 and GB1-16 are closest to shore, their sustained ^{234}Th deficits may have been influenced by lateral advection of particles from the continental shelf. At these stations, $z_{Th/U}$ depths were approximated by the depth below which ^{234}Th activities remain constant with depth. For example, at station GB1-6, $z_{Th/U}$ = 130 m because below this depth ^{234}Th activities remained relatively constant.

In the Atlantic sector, sampled in January – February 2011, all observed z_{PAR} depths were significantly shallower than $z_{Th/U}$ depths (Student's t-test $p<0.05$); on average, z_{PAR} was 66 ± 44 % shallower than $z_{Th/U}$. By contrast, in the Indian sector, sampled roughly a year later in February – March 2012, z_{PAR} was not significantly different from $z_{Th/U}$ ($p>0.05$), and the average relative difference was -6 ± 29%. In general, when water-column ^{234}Th activity is at steady-state, the euphotic zone should correspond to the region of ^{234}Th deficit relative to ^{238}U (Buesseler et al., 2008; Buesseler and Boyd, 2009), i.e., z_{PAR} should equal $z_{Th/U}$.

Using integrated activity deficits, export fluxes of ^{234}Th, POC, PIC, and BSi at z_{PAR} were estimated at the 27 sites (Figs. 5, 6; Table 3). Overall mean ^{234}Th fluxes at z_{PAR} were 1,413 ± 432 dpm m^{-2} d^{-1} (mean ± 1 s.d.), and ranged from 717 to 2,437 dpm m^{-2} d^{-1} at stations GB2-112 and GB1-6, respectively. Mean derived POC fluxes at z_{PAR} were 4.5 ± 3.9 mmol m^{-2} d^{-1}, ranging from 0.97 to 20 mmol m^{-2} d^{-1} at stations GB2-112 and GB1-85, respectively. Mean PIC fluxes were 1.2 ± 1.7 mmol m^{-2} d^{-1}, and ranged from 0.067 to 6.2 mmol m^{-2} d^{-1} at stations GB2-73 and GB1-59, respectively. Finally, mean BSi fluxes at z_{PAR} were 3.8 ± 5.8 mmol m^{-2} d^{-1}, ranging from 0.17 to 28 mmol m^{-2} d^{-1}at stations GB2-46 and GB1-85, respectively. Higher POC export stations frequently corresponded with higher BSi export stations (e.g., station GB1-85), but less so with higher PIC export stations.

The highest and lowest measured biomineral (PIC and BSi) fluxes at z_{PAR} were in GB1 and GB2, respectively, but mean values were not significantly different between ocean basins because of high variability within each basin (Fig. 6). However, mean POC

fluxes at z_{PAR} were significantly higher in GB1 (mean ± 1 s.d.= 6.0 ± 4.9 mmol m^{-2} d^{-1}) than in GB2 (3.0 ± 1.7 mmol m^{-2} d^{-1}) (Student's t-test $p>0.05$). Because POC:^{234}Th values did not differ between GB1 and GB2 ($p<0.05$), we attribute this inter-basin difference in POC fluxes primarily to significantly higher ^{234}Th fluxes in GB1 (1,574 ± 463 dpm m^{-2} d^{-1}) relative to fluxes in GB2 (1,240 ± 330 dpm m^{-2} d^{-1}).

Further, there were significant latitudinal differences among export fluxes and particulate composition ratios in three temperature/nutrient regimes across both sectors (Fig.1; Table 4): (1) north of 45° S, the approximate location of the Subantarctic front, where temperatures exceeded ~10°C; (2) south of 52 °S, the approximate location of the Polar Front (e.g., Belkin and Gordon, 1996; Sokolov and Rintoul, 2009), where temperatures remained below ~5°C; and (3) between 45° S and 52 °S, where temperatures ranged from ~5-10 °C. The >51 μm size-fraction POC:^{234}Th values at z_{PAR} were significantly lower in the most equatorward zone north of 45 °S, where average ratios were 1.9 ± 0.9 μmol dpm^{-1}. The highest average ratios, south of 52°S, were 5.4 ± 3.0 μmol dpm^{-1}, illustrating the wide variation in POC:^{234}Th ratios with ecosystem type (Buesseler et al., 2006; Jacquet et al., 2011). Likewise, zonally averaged POC export fluxes in the most equatorward zone (2.7 ± 2.3 mmol m^{-2} d^{-1}) were significantly lower than average fluxes in the most poleward zone (8.0 ± 6.3 mmol m^{-2} d^{-1}). BSi:^{234}Th values were significantly different in all three zones, with highest average ratios south of 52°S (7.1 ± 4.1 μmol dpm^{-1}) and smallest ratios north of 45°S (0.3 ± 0.1 μmol dpm^{-1}). Similarly, average BSi export fluxes were also significantly different from each other in all three zones, with the greatest average values south of 52°S (10 ± 8.7 mmol m^{-2} d^{-1}), and lowest values north of 45°S (0.35 ± 0.16 mmol m^{-2} d^{-1}). Finally, PIC:^{234}Th ratios, which averaged 0.72 ± 0.85 μmol dpm^{-1} across all zones, and PIC export fluxes were not significantly different from each other in any zone defined by these latitudinal bands.

These fluxes are sensitive to the choice of export depth (z_{PAR} or $z_{Th/U}$), not only because the export depth determines the magnitude of ^{234}Th flux by influencing the integrated ^{234}Th deficit, but also because the export depth determines which POC:^{234}Th ratio best describes particles sinking from the chosen depth (Fig. S1). Across stations, the depth metrics z_{PAR} and $z_{Th/U}$ differed from each other to varying extents (Fig. 4; Table 1). As exemplified by stations GB1-92, GB1-16, and GB2-100, POC fluxes changed

significantly between z_{PAR} and $z_{Th/U}$ (Figs. 5b, 5c; Table S2). At station GB1-92, where z_{PAR} was 40 m shallower than $z_{Th/U}$, POC flux decreased from 8.0 mmol m^{-2} d^{-1} at z_{PAR} to 5.1 mmol m^{-2} d^{-1} at $z_{Th/U}$. In contrast, at station GB1-16, where z_{PAR} was 80 m shallower than $z_{Th/U}$, POC fluxes increased from 5.9 mmol m^{-2} d^{-1} to 6.6 mmol m^{-2} d^{-1}. At station GB2-100, one of few stations where z_{PAR} was deeper than $z_{Th/U}$, POC fluxes decreased from 3.3 to 1.5 mmol m^{-2} d^{-1} going deeper. At this station, the POC:^{234}Th ratio at $z_{Th/U}$ was 102% greater than ratios at z_{PAR}, while ^{234}Th fluxes at $z_{Th/U}$ were 6% greater than fluxes at z_{PAR}, demonstrating that changes in particle composition disproportionately contributed to the observed difference in POC export at z_{PAR} and $z_{Th/U}$. By contrast, at station GB1-16, the relative change in ^{234}Th fluxes from z_{PAR} to $z_{Th/U}$ (+29%) contributed more to the increase in POC flux with depth than the relative change in POC:^{234}Th ratio (-13%). Finally, for station GB1-92, the relative change in ^{234}Th flux with depth (-19%) was similar to the relative change in POC:^{234}Th with depth (-21%), demonstrating that the export flux estimate was equally sensitive to changes in both parameters.

4 Discussion

The following discusses these flux measurements in the context of other Southern Ocean observations, and hypotheses surrounding the transformation of sinking organic carbon within the euphotic and mesopelagic zones of the water column.

4.1 Choice of export depth

The two possible depths we use to calculate export flux, z_{PAR} and $z_{Th/U}$, are significantly different in the Atlantic sector, which influences the magnitude of flux estimated (see Sect. 3). We offer here two possible and not mutually exclusive explanations for why $z_{Th/U}$ depths were on average deeper than z_{PAR} depths at GB1 stations.

One hypothesis is that the ^{234}Th - ^{238}U profiles used to calculate export fluxes may not have been at steady-state during the time of sampling on the GB1 cruise. Non-steady state conditions in the ^{238}U-^{234}Th system do occur during phytoplankton blooms,

particularly during their decline and ascent (Savoye et al., 2006; Buesseler et al., 2009). For example, a recent and rapid increase in the near-surface particle concentration could decrease the depth of light penetration faster than the ^{238}U-^{234}Th system can adjust, leading to a z_{PAR} measured on station that is shallower than the $z_{Th/U}$, which reflects conditions prior to the rapid increase. Since the GB1 cruise in the Atlantic sector took place a month earlier in the growing season (January-February 2011) than the GB2 cruise in the Indian sector (February-March 2012), the two sectors may have been sampled at different stages of the seasonal bloom, contributing to differences in agreement between z_{PAR} and $z_{Th/U}$. Satellite chlorophyll time-series, if well-resolved, can shed light on how dynamic primary production was around the time of sampling at each station of GB1 and GB2, whether rapid (i.e., within three weeks) changes in particle production and sinking fluxes from a bloom could have decoupled ^{234}Th-^{238}U deficits from light profiles into the surface ocean of the Great Calcite Belt. Eight-day composites of chlorophyll imagery from December 2010 to February 2011 were required to overcome spatial patchiness in the data due to clouds, and indicate that the changes leading up to sampling during GB1 were not consistent across all stations where $z_{PAR} < z_{Th/U}$. At several stations, chlorophyll concentrations declined towards the sampling date; at others, chlorophyll did not change or increased towards the sampling date. Moreover, out of the three stations where $z_{PAR} = z_{Th/U}$, only one exhibited relatively constant chlorophyll concentrations in the month preceding sampling. In GB2, where the differences between z_{PAR} and $z_{Th/U}$ were not significant, chlorophyll tended to be constant preceding more sampling stations. Nonetheless, as in GB1, several locations still experienced increasing or decreasing chlorophyll concentrations in the weeks before sampling, despite having a similar z_{PAR} and $z_{Th/U}$.

The inability of the chlorophyll time-series to unequivocally resolve the differences between z_{PAR} and $z_{Th/U}$ points to other possible mechanisms underlying the discrepancy. One other mechanism, which does not necessarily preclude non-steady state in the ^{234}Th system, is sinking particle production below the euphotic zone z_{PAR} (Trull et al., 2008). Physical aggregation and fecal pellet production by zooplankton grazing in the region below z_{PAR} (i.e., the upper mesopelagic zone) can increase the speed and total abundance of sinking of particles by transforming phytoplankton biomass exiting the

euphotic zone, thereby contributing to sustained ^{234}Th deficits below z_{PAR} (Steinberg et al., 2008; Wilson et al., 2008; Abramson et al., 2010). Why this occurs only in GB1 and not GB2 is not known.

For example, the ~70m difference in z_{PAR} and $z_{Th/U}$ at a station like GB1-85 (Table 1) may be attributed to additional production or repackaging of sinking particles in the upper mesopelagic zone, causing ^{234}Th deficits to persist beyond the euphotic zone of primary productivity, and a deeper $z_{Th/U}$. Images of >51 μm particles from this station highlight the changing nature of >51 μm particles with depth (Fig. 2), from primarily large phytoplankton in the euphotic zone to predominantly fecal pellets in the mesopelagic zone. The difference in POC fluxes measured at both depths may arise from the evolution of these particles during vertical transit, from predominantly intact and relative buoyant diatoms at z_{PAR} to degraded, sinking fecal pellets produced between z_{PAR} and $z_{Th/U}$.

Going forward, it is most important to keep in mind how the choice of export depth impacts flux estimates. For this study, all export fluxes are defined by z_{PAR} so that they can be compared with integrated primary production measurements (Buesseler and Boyd, 2009). Non-steady-state effects of ^{234}Th profiles on export fluxes will not be considered further because we do not have Lagrangian observations at multiple time points necessary to detect such effects (Buesseler et al., 2003; Resplandy et al., 2012).

4.2 Comparison of export fluxes to previous studies

The ^{234}Th fluxes we report (mean ± S.D.= 1,413 ± 432 dpm m^{-2} d^{-1}) are generally within range of measurements from other Southern Ocean studies (1,615 ± 1,050 dpm m^{-2} d^{-1}) (compilation by Le Moigne et al., 2013: Shimmield et al., 1995; Rutgers Van Der Loeff et al., 1997; Buesseler, 1998; Cochran et al., 2000; Buesseler et al., 2001; Friedrich and van der Loeff, 2002; Buesseler et al., 2003; Coppola et al., 2005; Morris et al., 2007; Thomalla et al., 2008; Savoye et al., 2008; Rodriguez y Baena et al., 2008; Jacquet et al., 2011; Rutgers van der Loeff et al., 2011; Zhou et al., 2012; Planchon et al., 2013). By contrast, the POC fluxes we report (4.5 ± 3.9 mmol m^{-2} d^{-1}) are on average three times lower than fluxes from other studies (12.6 ± 13.3 mmol m^{-2} d^{-1}) due to lower POC:^{234}Th

469 ratios measured in >51 μm particles. In general, POC:^{234}Th ratios can vary widely as a
470 function of season, ecosystem composition, size-fraction, depth, and particle sampling
471 methodology (Coppola et al., 2005; Buesseler et al., 2006; Santschi et al., 2006; Jacquet
472 et al., 2011). In GB1 and GB2, an ecosystem effect likely accounts for the 14-fold
473 difference in POC:^{234}Th between oligotrophic waters (e.g, 0.8 μmol dpm^{-1} at GB2-106)
474 and polar waters (e.g., 10.8 μmol dpm^{-1} at GB1-85) (Table 3). The Le Moigne et al.
475 (2013) dataset may include more studies from diatom-rich ecosystems with high
476 POC:^{234}Th organic particles, such as observed by Buesseler (1998; not included in Le
477 Moigne et al. 2013), driving some of the discrepancy between our observations and POC
478 fluxes reported by (Le Moigne et al., 2012).
479 Other potential reasons for POC:^{234}Th differences are the choice of export depth
480 (see Sect. 4.1) and different sampling methodologies in the previous studies. For instance,
481 in-situ pump filter holders with a small-diameter central intake and thus higher intake
482 velocities have been observed to sample more zooplankton, which typically have higher
483 POC:^{234}Th ratios, than filter holders with diffuse intakes (Bishop et al., 2012). This is
484 because swimming zooplankton can avoid the gentle intake velocities of filter holders
485 with diffuse intakes but not the higher velocities of small diameter intakes. This would
486 be expected to affect estimates of ^{234}Th-derived POC flux more than ^{234}Th-derived
487 biomineral fluxes.
488 There have been far fewer estimates of ^{234}Th-derived biomineral export fluxes
489 (Thomalla et al., 2008; Sanders et al., 2010; Le Moigne et al., 2012; Le Moigne et al.,
490 2013). BSi and PIC fluxes observed during GB1 and GB2 are within the range
491 previously observed during the *Crozex* study by the Crozet islands (Le Moigne et al.,
492 2012), the site of station GB2-27. Thomalla et al. (2008) also reported biomineral fluxes
493 from the Atlantic Meridional Transect (AMT), north of the Subantarctic Front. While
494 AMT PIC export fluxes were only two times smaller than our mean PIC fluxes in the
495 Great Calcite Belt region, AMT BSi fluxes were ten times smaller. The disparity in BSi
496 fluxes is unsurprising, since the AMT cruise track was through waters with low
497 abundance of silicifiers. We also find that the PIC and BSi fluxes from our Great Calcite
498 Belt study are 4 and 10 times larger than biomineral fluxes estimated by Henson et al.
499 (2012b), respectively, who used a steady-state model of nutrient uptake against nutrient

export (Sarmiento et al., 2002; Sarmiento et al., 2004). The Henson et al. method used annual climatologies of nutrient concentration profiles for their estimates, whereas the ^{234}Th-derived export method used here integrates over several weeks in the growing season. This difference in timescales of integration likely accounts for the smaller biomineral fluxes in Henson et al. (2012b).

4.3 Export efficiency

We found no significant relationship observed between integrated primary productivity and POC flux at z_{PAR}, highlighting the variable export efficiency across GB1 and GB2. Export efficiencies, or "Ez-ratios" (Buesseler and Boyd, 2009), were calculated as the ratio of POC flux at z_{PAR} to total integrated primary production in the euphotic zone (Fig. 7b; Table 3). Mean export efficiencies were 0.26 ± 0.19, and ranged from 0.04 to 0.77 at stations GB1-16 and GB2-63, respectively. The lack of association between primary productivity and POC export flux confirms previously observed decoupling between the factors that drive export and those that modulate primary productivity (Buesseler et al., 2001; Coppola et al., 2005; Maiti et al., 2012).

4.4 Vertical attenuation of POC flux and concentration

At most stations, both POC flux and >51 μm [POC] decline with depth below z_{PAR} as a result of remineralization. In the following, we use two metrics to describe POC transfer in the mesopelagic zone: (1) the attenuation of >51um [POC] in the mesopelagic zone, expressed as the attenuation coefficients extracted from power-law fits of mesopelagic >51 μm [POC] (exponent from Eq. (1)) and (2) the POC flux transfer efficiency (T_{100}), defined as the fraction of ^{234}Th-based POC flux that survives remineralization and is transferred 100 m below z_{PAR} (Buesseler and Boyd, 2009). The first metric describes the disappearance of POC concentration, and applies to the entire mesopelagic zone; the second metric describes the survival of POC flux, and applies to the upper mesopelagic zone.

The mean T_{100} was 0.71 ± 0.38, ranging from 0.20 to 1.8 at stations GB2-119 and GB1-25, respectively (Fig. 7c**;** Table 2), generally falling within the spread of values observed globally as well as specifically in the Southern Ocean (Buesseler and Boyd, 2009). At stations GB1-6, GB1-16, GB1-25, GB1-59, and GB2-106, T_{100} values are greater than 1.0 and reflect an increase in POC flux with depth between z_{PAR} and 100 m below z_{PAR} (Figs. 5b, 5d). Transfer efficiencies greater than 1 can occur during a declining bloom (Henson et al., 2015), but examination of satellite chlorophyll time-series does not indicate that these stations were sampled at such conditions. At GB1-6, GB1-16 and GB1-59, the ^{234}Th-^{238}U disequilibrium extends relatively deep (>200m) into the water column, thus leading to continually increasing ^{234}Th flux with depth, suggesting that either renewed particle production at depth or lateral advection of particles away from these coastal stations could sustain the ^{234}Th deficit below z_{PAR}. Moreover, because z_{PAR} depths are significantly shallower than $z_{Th/U}$ in most GB1 stations, including GB1-6, GB1-16 and GB1-59, the transfer efficiency calculation at these stations in GB1 captures an increase in ^{234}Th flux between z_{PAR} and 100 m below z_{PAR}. Thus, for the following discussion, it is important to view transfer efficiency values with the caveat that GB1 and GB2 stations display different ^{234}Th-^{238}U disequilibria profiles with respect to z_{PAR} and $z_{Th/U}$, and this difference impacts all calculations that use a ^{234}Th flux component.

At the two other stations for which T_{100}>1, GB1-25 and GB2-106, the increases in POC flux below z_{PAR} arise primarily from increasing POC:^{234}Th ratios rather than increasing ^{234}Th flux with depth (Figs. S1a, S1d). The increase in these ratios results from a faster decrease in particulate ^{234}Th activity compared to changes in >51 μm [POC] with depth. This is unexpected and at all other stations, >51 μm [POC] decreases more quickly than particulate ^{234}Th activity due to organic carbon remineralization. We suspect that poor >51 μm particle distribution on filters from GB2-106 may have led to anomalously low POC around z_{PAR}, but do not have an explanation for the consistent increase in POC:Th with depth at GB1-25 (Figs. S1a). We proceed by excluding the T_{100} transfer efficiencies from these two stations from statistical tests, but identify them for completeness (Figs. 7, 9).

The general decline in POC flux with depth at most stations is mirrored by a decrease in >51 μm [POC], both of which are a result of remineralization. Attenuation

coefficients from power-law fits of mesopelagic >51 μm [POC] at 22 stations describe this transformation from z_{PAR} to the lower mesopelagic zone, where >51 μm [POC] between 800-1000 m was 1.5 to 137 times lower than >51 μm [POC] at z_{PAR} (Figs. 8b, 8c; Table 2). We discount the attenuation value at station GB2-93 from discussion because it had an anomalously low >51 μm [POC] at 800m, likely due to incomplete rinsing of particles from the prefilter. This drove the power law fit to yield an anomalously high attenuation coefficient, an outlier, as approximated by Chauvenet's Theorem (Glover et al., 2011). Attenuation coefficients were 1.1 ± 0.50 on average, and varied from 0.4 to 1.9 at stations GB1-25 and GB2-43, respectively (Fig. 8c; Table 2), which spans the global range compiled by Lam et al. (2011).

The >51 μm [POC] at z_{PAR} is not correlated with >51 μm [POC] at lower mesopelagic depths, suggesting that processes controlling >51 μm [POC] at the top of the mesopelagic differ from those controlling >51 μm [POC] at the base of the mesopelagic zone. This is supported by the great variation in attenuation coefficients and transfer efficiencies, and suggests that POC concentrations at z_{PAR} are decoupled from [POC] at z ≥800m, as has also been noted in other POC flux and concentration observations (Lomas et al., 2010; Lam et al., 2011; Henson et al., 2012b). There are some exceptions, such as at GB1-85, which exhibited the highest >51 μm [POC] both at z_{PAR} and below 800 m, but there is no overall relationship across the dataset. The remaining discussion aims to tease apart the processes that control POC flux and >51 μm [POC] in each depth regime.

4.5 Biomineral-POC flux correlations at z_{PAR}

We compared POC fluxes to mineral fluxes at z_{PAR} (Figs. 9a, 9b) to test the hypothesis that mineral ballasting facilitates POC export out of the euphotic zone, as has been observed in deeper flux datasets >1000 m (Klaas and Archer, 2002; Armstrong et al., 2002; Francois et al., 2002). Because we use ^{234}Th activity deficits and the same particulate ^{234}Th activities to derive all fluxes (Eq. (4-6)), comparing export fluxes is equivalent to comparing concentrations of >51 μm POC, BSi and PIC at z_{PAR}. In this dataset, minor differences between flux versus concentration comparisons (not shown)

591 arise from differences in interpolation methods for POC:^{234}Th, BSi:^{234}Th, and PIC:^{234}Th
592 ratios at z_{PAR} (Table 3).
593 Pearson correlation tests between shallow POC export and the two biomineral
594 fluxes revealed a significantly positive correlation between POC and BSi fluxes
595 ($p<<0.001$, $r^2=0.77$). By contrast, there was no significant relationship between shallow
596 POC and PIC fluxes ($p=0.24$, $r^2=0.06$). Both BSi and POC export fluxes tend to increase
597 poleward from the region north of the Subtropical/Subantarctic fronts to the inter-frontal
598 zone to the region south of the Polar front (Figs. 5b, 6a, 6b). Station GB1-85, which sits
599 just south of the Polar Front (~52°S), is a high BSi and POC flux outlier. When removed,
600 the BSi flux vs. POC flux correlation remains significant, though weaker ($r^2= 0.43$),
601 suggesting that although this correlation is strongly influenced by station GB1-85, the
602 shallow BSi ballast association still remains valid for the rest of the dataset.
603 We also compared POC export fluxes to both PIC and BSi export fluxes
604 simultaneously by multiple linear regression:
605 $$\text{POC Flux} = (m_{\text{BSi}} \times \text{BSi Flux}) + (m_{\text{PIC}} \times \text{PIC Flux}) + \text{constant} \quad (7)$$
606 The multiple linear regression only explains an additional 5% of the variance in POC flux
607 at z_{PAR} ($r^2=0.82$, $p<< 0.001$), affirming that BSi flux explains most of the variation in
608 POC export fluxes at z_{PAR} across the Atlantic and Indian sectors of the Great Calcite Belt
609 region.
610 The per-mole carrying capacities of BSi and PIC for POC, or the slopes m_{BSi} and
611 m_{PIC} in the multiple linear regression Eq. (7), are 0.60 and 0.50, respectively. The per-
612 weight carrying capacities of BSi and PIC for POC are 0.23 and 0.13, respectively,
613 assuming 12 x 2.199 g mol^{-1} POC, 67.3 g $SiO_20.4H_2O$ mol^{-1} BSi and 100.1 g $CaCO_3$
614 mol^{-1} PIC (Klaas and Archer 2002). The unassociated POC flux, the constant in Eq. (7),
615 is 1.7 mmol POC m^{-2} d^{-1}, or 44 mg POC m^{-2} d^{-1}. These carrying capacities for POC are 2-
616 10 times higher than global biomineral carrying capacities of deeper (>2000m) flux data
617 (m_{BSi}=0.025-0.026, m_{PIC}=0.070-0.074; Klaas and Archer, 2002), reflecting how POC
618 remineralization with depth consistently reduces apparent mineral carrying capacities
619 between the base of the euphotic zone and the deep sea.
620 These upper ocean carrying capacities, especially m_{PIC}, are considerably different
621 than corresponding per-weight carrying capacities reported in the *Crozex* study in the

Indian sector of the Southern Ocean (m_{BSi}= 0.16, m_{PIC}= -0.11, constant=105 mg POC m^{-2} d^{-1}) (Le Moigne et al., 2012). But, as the *Crozex* study was carried out several months earlier in the growing season than our sampling of the same area within the Great Calcite Belt, seasonal changes in the phytoplankton communities and their associated food webs could account for the differences in upper ocean carrying capacities. The Le Moigne et al. (2012) study also highlighted that variable ecosystem composition contributed to regional variations in upper ocean carrying capacities (Le Moigne et al. 2014), echoing a contemporaneous study that showed that even the deep (>1500 m) flux carrying capacities have statistically significant spatial variability (Wilson et al., 2012).

It is worth noting that Le Moigne et al. (2012) included lithogenic minerals in their multiple linear regressions. We did not measure lithogenic minerals on GB1 and GB2, as we assumed lithogenic fluxes to be small in the Southern Ocean due to low terrestrial dust inputs (e,g., Honjo et al., 2000). While omitting this lithogenic component from the multiple linear regression could potentially impact derived m_{BSi} and m_{PIC} values, lithogenic material is nonetheless unlikely to be an important carrier of POC flux because of its low flux in the Southern Ocean. Indeed, regional studies have found that the lithogenic carrying capacity (Wilson et al., 2012) and the lithogenic-associated POC fluxes (Le Moigne et al., 2012) are very low in the Southern Ocean.

4.6 Mineral-POC flux correlations in the mesopelagic zone

To directly test whether minerals facilitate POC transfer through the upper mesopelagic zone of the water column as well, we compared flux transfer efficiencies 100 m below the base of the euphotic zone (T_{100}) with BSi and PIC fluxes at z_{PAR} (Figs. 9c, 9d). If the mineral ballast model were to apply to the upper mesopelagic zone, one would expect greater transfer efficiencies (i.e., lower attenuation of POC flux) in regions of higher mineral export. The data highlight several key differences between the role of minerals in the euphotic and upper mesopelagic zones. For one, the correlation between PIC flux and T_{100} , excluding values at GB1-25 and GB2-106, is significantly positive ($p<0.001$, $r^2=0.39$). The relationship remains even when assessing data from each cruise

individually (for GB1, p=0.047, r^2= 0.34; for GB2, p= 0.009, r^2=0.52), lending further support to a potential role for PIC in POC transfer through the upper mesopelagic zone.

Further, there was no significant correlation, with or without GB1-25 and GB2-106 T_{100} values, between BSi export fluxes in GB2 and T_{100}. However, higher particulate biogenic silica concentrations (>51 μm [BSi]) at z_{PAR} did correspond with greater attenuation of >51 μm [POC] below z_{PAR} (p=0.004, r^2=0.35; Fig. 10a), suggesting that in contrast to its role in the euphotic zone, BSi is associated with greater degradation in the mesopelagic zone of the water column.

4.7 Other controls on POC transfer

The correlation between the attenuation of >51 μm [POC] and the size fractionation of POC (% >51 μm [POC]) at z_{PAR} is even stronger than with >51 μm [BSi] (p<<0.001, r^2=0.63; Fig. 10b). GB1-85 appears to be an outlier for both relationships in Fig. 10, but especially for the relationship between >51 μm [POC] attenuation and >51 μm [BSi] (Fig. 10a). The correlation remains significant when the high [BSi] value from station GB1-85 is removed. Notably, the power law fit at GB1-85 is not very good in the upper mesopelagic; fitting >51 μm [POC] between z_{PAR} and 500 m yields a better fit (higher r^2; see Fig. 3) with a higher attenuation coefficient of 2.35 (compared to 1.7 for the entire mesopelagic zone). This modified upper mesopelagic attenuation at GB1-85 improves the overall correlations between the attenuation coefficient and both >51 μm [BSi] (p<<0.001, r^2=0.60) and % >51 μm [POC] (p<<0.001 ; r^2=0.78), further strengthening the argument that >51 μm [BSi] and % >51 μm [POC] at z_{PAR} are important factors in POC transfer in the upper mesopelagic zone.

The relationships between the attenuation of >51 μm [POC] and >51 μm [BSi] and particle size fractionation may arise from a more fundamental feature shared by both high-[BSi] and large-particle stations of the Great Calcite Belt: diatom-rich phytoplankton communities. Indeed, we also observe a strong correlation between >51 μm [BSi] and % >51 μm [POC] at z_{PAR} (p<<0.001, r^2= 0.65; not shown). This is a consistent feature across diatom-rich populations, which produce large, BSi-rich organic aggregates that sink rapidly out of the euphotic zone (Michaels and Silver, 1988;

683 Buesseler, 1998; Thomalla et al. 2006). Indeed, euphotic zone diatom abundances
684 enumerated with a FlowCam® are significantly correlated with >51 μm [BSi] at zPAR at
685 corresponding stations in GB1 and GB2 (see supplement; Fig. S2a). Thus, characteristics
686 describing ecosystem structure may underlie the correlation between BSi export and POC
687 export in the Great Calcite Belt (Francois et al. 2002; Thomalla et al., 2008; Henson et
688 al., 2012a; Henson et al., 2012b).
689 However, ecosystem composition does not directly explain why larger particles
690 exported into the mesopelagic zone are remineralized more vigorously hundreds of
691 meters below (Fig. 10b). It is paradoxical that the same large particles that sink quickly
692 out of the euphotic zone would then remineralize faster, as well. This association between
693 attenuation coefficient and particle size suggests that these particles sink more slowly
694 than expected in the mesopelagic zone given their size (for example, as a result of high
695 porosity and low excess density), and/or that they are subject to faster remineralization
696 compared to regions with more POC in the small size fraction. Francois et al. (2002)
697 noted a negative relationship between bathypelagic transfer efficiency and opal flux, and
698 attributed this to increased lability in large diatom aggregates. Though we do not observe
699 any negative correlation between upper mesopelagic transfer efficiency (T_{100}) and BSi
700 fluxes at z_{PAR}, we suggest that potentially higher degradability of POC produced by
701 diatom-rich communities may similarly explain the relationship between particle size and
702 >51 μm [POC] attenuation in the upper mesopelagic zone.
703 The view of POC quality as a driving factor behind POC transfer argues for a
704 deterministic role of euphotic zone community structure in POC transfer below the
705 euphotic zone. It supports the conventional perspective that diatom-dominated
706 communities are strong exporters of large, sinking POC particles out of the euphotic zone
707 (Buesseler, 1998; Guidi et al., 2009), but also adds to the growing view that these
708 communities have poor transfer efficiency and high attenuation through the mesopelagic
709 zone (Francois et al., 2002; Guidi et al., 2009; Henson et al., 2012b; Henson et al.,
710 2012a).
711 For instance, station GB1-85, with over half of [POC] in the >51 μm size class
712 fraction in the euphotic zone (Fig. 6c; Table 3), has a low >51 μm [PIC]:[BSi] ratio of
713 0.035 at z_{PAR} (indicated in log-scale in Figs. 10a and 10b**)**, which indicates relatively high

714 diatom populations producing large BSi-rich aggregates (Figs. 2, S2, S3). Station GB1-85
715 exhibits a high export efficiency (Ez-ratio= 0.38, within the upper quartile of the data
716 set), and the highest >51 μm [POC] and export fluxes at z_{PAR} (Figs. 5b, 7b, 8a; Table 3).
717 Notably, >51 μm [POC] values in the lower mesopelagic zone are also the highest at
718 GB1-85, despite attenuating greatly below zPAR (attenuation coefficient = 1.7) (Figs. 3,
719 8b, 8c; Table 2). But, because of high attenuation, proportionally less organic carbon
720 transfers to the deep sea at GB1-85. The same diatom-rich communities that vigorously
721 export POC ultimately may not sequester as much organic carbon in the deep ocean or
722 draw down as much atmospheric CO_2 (Kwon et al., 2009) as would be expected
723 considering the magnitude of export alone.
724 In contrast to a model diatom community like station GB1-85, station GB1-25 is
725 BSi-deplete, with a >51 μm [PIC]:[BSi] ratio of 1.4 at z_{PAR} (indicated in log-scale in Fig.
726 10a), indicating relatively more coccolithophores in the community (Figs. S2, S3). With
727 proportionally less POC in the >51 μm size-fraction (only 3.2%) (Figs. 6c, 10b; Table 3),
728 >51 μm [POC] at GB1-25 attenuates little through the mesopelagic zone (attenuation
729 coefficient = 0.4, the lowest of the data set) such that a third of the >51 μm [POC] at z_{PAR}
730 remains at 1000m, compared to only 1.4% at station GB1-85 (Fig. 3). At GB1-25, export
731 efficiency is very low (Ez-ratio=0.04), suggesting that the particles exiting the euphotic
732 zone here have been recycled vigorously in the euphotic zone prior to export, which may
733 explain their low >51 μm [POC] and high proportion in the <51 μm size-fraction at z_{PAR}.
734 In the mesopelagic zone, these particles are not very reactive and thus remineralize very
735 little, perhaps sequestering a higher proportion of the CO_2 fixed in the euphotic zone.
736 Several other stations with proportionally more small particles and weaker >51
737 μm [POC] attenuation in the mesopelagic zone exhibit higher >51 μm [PIC] than >51 μm
738 [BSi] at z_{PAR} (labeled in the lower left quadrant of Fig. 10b), suggesting that export
739 regimes characterized by high relative abundance of coccolithophores consistently
740 transfer less reactive POC to the mesopelagic zone. Artificial roller tank experiments
741 have demonstrated that coccolithophore cultures can produce smaller, more compact
742 aggregates than diatom cultures, partly because of smaller cell sizes (Iversen and Ploug,
743 2010). However, smaller size does not necessarily mean slower sinking velocities (e.g.,
744 McDonnell and Buesseler, 2010). Iversen and Ploug (2010) showed that the higher

745 excess density of these small aggregates generated faster sinking speeds than similarly
746 sized pure diatom aggregates. Another roller tank study that compared aggregate
747 formation by calcifying versus non-calcifying coccolithophores observed that aggregates
748 formed from calcifying coccolithophores were smaller but faster sinking (Engel et al.,
749 2009). In regions like the Great Calcite Belt, dense coccolithophore populations may
750 similarly export small, highly degraded and compact particles out of the euphotic zone.
751 As a result, these communities would efficiently transfer POC towards the base of the
752 mesopelagic zone, even if the magnitude of exported POC is not as high as in diatom-rich
753 regions (Thomalla et al., 2008; Guidi et al., 2009; Henson et al., 2012b). This may
754 explain why higher PIC export fluxes are associated with higher transfer efficiencies but
755 not higher POC flux at z_{PAR} (Fig. 9), and also why the ballast association between PIC
756 and POC fluxes appears only at greater depths (Francois et al., 2002; Klaas and Archer,
757 2002).

758 Attenuation coefficients for >51 μm [POC] across diatom-rich regions exhibit a
759 great spread (standard deviation= 0.47), ranging from 0.47 to 1.88. Not all diatom-rich
760 stations (i.e., >51 μm [PIC]:[BSi]<1 at z_{PAR}) have proportionally larger particles or higher
761 b-values (e.g., stations GB1-70, GB1-77 and GB2-87; Fig. 10b). In contrast, attenuation
762 coefficients across coccolithophore-rich regions (i.e., >51 μm [PIC]:[BSi] ≥ 1 at z_{PAR})
763 exhibit a lower standard deviation (0.31) and a smaller range, 0.35 to 1.12. The greater
764 variance in attenuation across BSi-rich regions may result from sampling the diatom
765 populations at different seasons of the bloom cycle (Lam et al., 2011), and implies that
766 there may be less seasonality in POC transfer to depth in coccolithophore-rich regions.
767 Indeed, massive diatom export events with high transfer efficiency through the
768 mesopelagic zone have been observed (Martin et al., 2011; Smetacek et al. 2012), so
769 there are clearly conditions that can lead to efficient mesopelagic POC transfer from
770 diatom blooms.

771 It is worth noting that >51 μm [PIC]:[BSi] ratios did increase with depth at most
772 stations of the Great Calcite Belt, as might be expected because BSi is undersaturated in
773 seawater. The possibility that BSi dissolves faster than PIC in particles sinking through
774 the mesopelagic zone would complicate the connections we draw between diatom-rich
775 communities in the euphotic zone and the attenuation of >51 μm [POC]. But, there are no

776 associations between the magnitude of [PIC]:[BSi] increase and >51 μm [BSi] at z_{PAR},
777 >51 μm [PIC] at z_{PAR} or >51 μm [POC] attenuation with depth, suggesting that the issue
778 of differential dissolution should not significantly impact our earlier interpretations. In
779 the future, directly evaluating the degradability of sinking POC using organic
780 characterization techniques (e.g., ramped pyrolysis or biomarker isolation) (e.g.,
781 Wakeham et al., 2002; Rosenheim et al., 2008; Rosenheim and Galy, 2012; Rosenheim et
782 al., 2013) would greatly improve our ability to track the transformation of POC produced
783 by different ecosystem assemblages across the Great Calcite Belt.
784
785 **5 Conclusion**
786
787 In summary, we argue here that phytoplankton assemblages play a fundamental
788 role (Francois et al., 2002; Thomalla et al., 2008; Henson et al., 2012b; Henson et al.,
789 2012a) in determining the fate of POC export through the Great Calcite Belt region, the
790 effect of which sometimes, but not always, appears as a mineral ballast mechanism in the
791 euphotic zone (Lam et al., 2011; Henson et al., 2012a; Lima et al., 2013). Though
792 shallow BSi export fluxes were strongly correlated with POC export fluxes, they are also
793 associated with diatom communities that produce larger particles that attenuate more
794 quickly through the mesopelagic zone, such that proportionally less POC reaches the
795 lower mesopelagic zone, and proportionally more is returned to the water column as
796 remineralized carbon (dissolved inorganic and organic carbon).
797
798 **Author contributions:**
799 S.Z. Rosengard, the primary author, participated in the GB2 field work, sample analysis
800 in lab and writing. P.J. Lam contributed to field work during GB2, and participated in
801 both data interpretation and editing the manuscript. W.M. Balch, supplied the primary
802 productivity and light profile data included here, and provided valuable feedback during
803 writing. M.E. Auro and S. Pike participated in field work and sample analysis during and
804 after GB1. D. Drapeau and B. Bowler contributed to field work during both GB1 and
805 GB2, as well as sample analysis, particularly with respect to primary productivity and
806 light profile data.

Acknowledgements:

Many thanks to Ken Buesseler for discussions and lending us field equipment; Dan Ohnemus, Angela Warner, Michael Brown, Rebecca Fowler, and Marina Van der Eb for help at sea; and Laura Lubelczyk, Paul Henderson, and Scott Birdwhistell for analytical work/assistance. This work was funded by NSF OCE-0960880 to P.J. Lam, and NSF OCE-0961660, NASA NNX11A072G and NNX11AL93G to W.M. Balch.

References

Abramson, L., Lee, C., Liu, Z. F., Wakeham, S. G., and Szlosek, J.: Exchange between suspended and sinking particles in the northwest Mediterranean as inferred from the organic composition of in situ pump and sediment trap samples, Limnology and Oceanography, 55, 725-739, 2010.

Armstrong, R. A., Lee, C., Hedges, J. I., Honjo, S., and Wakeham, S. G.: A new, mechanistic model for organic carbon fluxes in the ocean based on the quantitative association of POC with ballast minerals, Deep-Sea Research Part Ii-Topical Studies in Oceanography, 49, 219-236, 2002.

Balch, W. M., Drapeau, D., and Fritz, J.: Monsoonal forcing of calcification in the Arabian Sea, Deep-Sea Research II, 47, 1301-1337, 2000.

Balch, W. M., Drapeau, D. T., Bowler, B. C., Lyczkowski, E. R., Lubelczyk, L. C., Painter, S. C., and Poulton, A. J.: Surface biological, chemical, and optical properties of the Patagonian Shelf coccolithophore bloom, the brightest waters of the Great Calcite Belt, Limnology and Oceanography, 59, 1715-1732, 2014.

Balch, W. M., Drapeau, D. T., Bowler, B. C., Lyczskowski, E., Booth, E. S., and Alley, D.: The contribution of coccolithophores to the optical and inorganic carbon budgets during the Southern Ocean Gas Exchange Experiment: New evidence in support of the Great Calcite Belt hypothesis, J. Geophys. Res., 116, C00F06, 2011a.

Balch, W. M., Poulton, A. J., Drapeau, D. T., Bowler, B. C., Windecker, L. A., and Booth, E. S.: Zonal and meridional patterns of phytoplankton biomass and carbon fixation in the Equatorial Pacific Ocean, between 110°W and 140°W, Limnology and Oceanography, 59, 1715-1732, 2011b.

Belkin, I. M. and Gordon, A. L.: Southern Ocean fronts from the Greenwich meridian to Tasmania, Journal of Geophysical Research: Oceans (1978–2012), 101, 3675-3696, 1996.

Bishop, J. K. B., Lam, P. J., and Wood, T. J.: Getting good particles: accurate sampling of particles by large volume in-situ filtration, Limnology and Oceanography Methods, 10, 681-710, 2012.

Brzezinski, M. A. and Nelson, D. M.: Seasonal changes in the silicon cycle within a Gulf Stream warm-core ring, Deep Sea Research Part A. Oceanographic Research Papers, 36, 1009-1030, 1989.

Buesseler, K., Lamborg, C. H., Cai, P., Escoube, R., Johnson, R., Pike, S., Masque, P., McGillicuddy, D., and Verdeny, E.: Particle fluxes associated with mesoscale eddies in the Sargasso Sea, Deep-Sea Research II, 55, 1426-1444, 2008.

Buesseler, K. O.: The decoupling of production and particulate export in the surface ocean, Global Biogeochemical Cycles, 12, 297-310, 1998.

Buesseler, K. O., Ball, L., Andrews, J., Cochran, J. K., Hirschberg, D. J., Bacon, M. P., Fleer, A., and Brzezinski, M.: Upper ocean export of particulate organic carbon and biogenic silica in the Southern Ocean along 170 degrees W, Deep-Sea Research Part II-Topical Studies in Oceanography, 48, 4275-4297, 2001.

Buesseler, K. O., Barber, R. T., Dickson, M. L., Hiscock, M. R., Moore, J. K., and Sambrotto, R.: The effect of marginal ice-edge dynamics on production and export in the Southern Ocean along 170 degrees W, Deep-Sea Research Part Ii-Topical Studies in Oceanography, 50, 579-603, 2003.

Buesseler, K. O., Benitez-Nelson, C. R., Moran, S. B., Burd, A., Charette, M., Cochran,

J. K., Coppola, L., Fisher, N. S., Fowler, S. W., and Gardner, W. D.: An assessment of particulate organic carbon to thorium-234 ratios in the ocean and their impact on the application of ^{234}Th as a POC flux proxy, Marine Chemistry, 100, 2006.

Buesseler, K. O. and Boyd, P.: Shedding light on processes that control particle export and flux attenuation in the twilight zone of the open ocean, Limnol, Oceanogr, 54, 1210-1232, 2009.

Buesseler, K. O., Lamborg, C. H., Boyd, P. W., Lam, P. J., Trull, T. W., Bidigare, R. R., Bishop, J. K. B., Casciotti, K. L., Dehairs, F., Elskens, M., Honda, M., Karl, D. M., Siegel, D. A., Silver, M. W., Steinberg, D. K., Valdes, J., Van Mooy, B., and Wilson, S.: Revisiting carbon flux through the ocean's twilight zone, Science, 316, 567-570, 2007.

Buesseler, K. O., Pike, S., Maiti, K., Lamborg, C. H., Siegel, D. A., and Trull, T. W.: Thorium-234 as a tracer of spatial, temporal and vertical variability in particle flux in the North Pacific, Deep Sea Research Part I: Oceanographic Research Papers, 56, 1143-1167, 2009.

Cochran, J. K., Buesseler, K. O., Bacon, M. P., Wang, H. W., Hirschberg, D. J., Ball, L., Andrews, J., Crossin, G., and Fleer, A.: Short-lived thorium isotopes (Th-234, Th-228) as indicators of POC export and particle cycling in the Ross Sea, Southern Ocean, Deep-Sea Research Part Ii-Topical Studies in Oceanography, 47, 3451-3490, 2000.

Coppola, L., Roy-Barman, M., Mulsow, S., Povinec, P., and Jeandel, C.: Low particulate organic carbon export in the frontal zone of the Southern Ocean (Indian sector) revealed by Th-234, Deep-Sea Research Part I-Oceanographic Research Papers, 52, 51-68, 2005.

907 De La Rocha, C. L., Nowald, N., and Passow, U.: Interactions between diatom
908 aggregates, minerals, particulate organic carbon, and dissolved organic matter:
909 Further implications for the ballast hypothesis, Global Biogeochemical Cycles,
910 22, 2008.
911
912 Engel, A., Szlosek, J., Abramson, L., Liu, Z., and Lee, C.: Investigating the effect of
913 ballasting by $CaCO_3$ in Emiliania huxleyi: I. Formation, settling velocities and
914 physical properties of aggregates, Deep Sea Research Part II: Topical Studies in
915 Oceanography, 56, 1396-1407, 2009.
916
917 Fabry, V. J. and Balch, W. M.: Direct measurements of calcification rates in planktonic
918 organisms., U. Riebeseil, V.J. Fabry, L. Hansson and J.-P. Gattuso (Editors),
919 Guide to Best Practices in Ocean Acidification Research and Data Reporting.
920 European Project on Ocean Acidification (EPOCA), Bremerhaven, Germany,
921 2010. 185-196, 2010.
922
923 Francois, R., Honjo, S., Krishfield, R., and Manganini, S.: Factors controlling the flux of
924 organic carbon to the bathypelagic zone of the ocean, Global Biogeochemical
925 Cycles, 16, 1087, doi:10.1029/2001GB001722, 2002.
926
927 Friedrich, J. and van der Loeff, M. M. R.: A two-tracer (Po-210-Th-234) approach to
928 distinguish organic carbon and biogenic silica export flux in the Antarctic
929 Circumpolar Current, Deep-Sea Research Part I-Oceanographic Research Papers,
930 49, 101-120, 2002.
931
932 Giering, S. L. C., Sanders, R., Lampitt, R. S., Anderson, T. R., Tamburini, C., Boutrif,
933 M., Zubkov, M. V., Marsay, C. M., Henson, S. A., Saw, K., Cook, K., and Mayor,
934 D. J.: Reconciliation of the carbon budget in the ocean/'s twilight zone, Nature,
935 507, 480-483, 2014.
936
937 Glover, D. M., Jenkins, W. J., and Doney, S. C.: Modeling methods for marine science.,

938 Cambridge University Press, New York, 2011.
939
940 Guidi, L., Stemmann, L., Jackson, G. A., Ibanez, F., Claustre, H., Legendre, L., Picheral,
941 M., and Gorsky, G.: Effects of phytoplankton community on production, size and
942 export of large aggregates: A world-ocean analysis, Limnology and
943 Oceanography, 54, 1951-1963, 2009.
944
945 Hedges, J. I. and Oades, J. M.: Comparative organic geochemistries of soils and marine
946 sediments, Organic Geochemistry, 27, 319-361, 1997.
947
948 Henson, S., Lampitt, R., and Johns, D.: Variability in phytoplankton community structure
949 in response to the North Atlantic Oscillation and implications for organic carbon
950 flux, Limnology and Oceanography, 57, 1591, 2012a.
951
952 Henson, S. A., Sanders, R., and Madsen, E.: Global patterns in efficiency of particulate
953 organic carbon export and transfer to the deep ocean, Global Biogeochem. Cycles,
954 26, GB1028, 2012b.
955
956 Henson, S. A., Sanders, R., Madsen, E., Morris, P. J., Le Moigne, F., and Quartly, G. D.:
957 A reduced estimate of the strength of the ocean's biological carbon pump,
958 Geophys. Res. Lett., 38, L04606, 2011.
959
960 Henson, S. A., Yool, A., and Sanders, R.: Variability in efficiency of particulate organic
961 carbon export: A model study, Global Biogeochem. Cycles, 29, GB004965, 2015.
962
963 Honjo, S., Francois, R., Manganini, S., Dymond, J., and Collier, R.: Particle fluxes to the
964 interior of the Southern Ocean in the Western Pacific sector along 170 degrees W,
965 Deep-Sea Research Part Ii-Topical Studies in Oceanography, 47, 3521-3548,
966 2000.
967
968 Iversen, M. H. and Ploug, H.: Ballast minerals and the sinking carbon flux in the ocean:

carbon-specific respiration rates and sinking velocity of marine snow aggregates, Biogeosciences, 7, 2613-2624, 2010.

Jacquet, S. H. M., Lam, P. J., Trull, T., and Dehairs, F.: Carbon export production in the subantarctic zone and polar front zone south of Tasmania, Deep Sea Research Part II: Topical Studies in Oceanography, 58, 2277-2292, 2011.

Klaas, C. and Archer, D. E.: Association of sinking organic matter with various types of mineral ballast in the deep sea: Implications for the rain ratio, Global Biogeochemical Cycles, 16, 1116-1129, 2002.

Kwon, E. Y., Primeau, F., and Sarmiento, J. L.: The impact of remineralization depth on the air-sea carbon balance, Nature Geoscience, 2, 630-635, 2009.

Lam, P. J. and Bishop, J. K. B.: High biomass, low export regimes in the Southern Ocean, Deep Sea Research Part II: Topical Studies in Oceanography, 54, 601-638, 2007.

Lam, P. J., Doney, S. C., and Bishop, J. K. B.: The dynamic ocean biological pump: Insights from a global compilation of particulate organic carbon, $CaCO_3$, and opal concentration profiles from the mesopelagic, Global Biogeochem. Cycles, 25, GB3009, 2011.

Lam, P. J., Ohnemus, D. C., and Auro, M. E.: Size-fractionated major particle composition and concentrations from the US GEOTRACES north Atlantic zonal transect, Deep Sea Research Part II: Topical Studies in Oceanography, 2014. 2014.

Le Moigne, F., Henson, S., Sanders, R., and Madsen, E.: Global database of surface ocean particulate organic carbon export fluxes diagnosed from the 234 Th technique, Earth System Science Data Discussions, 6, 163-187, 2013.

Le Moigne, F. A. C., Pabortsava, K., Marcinko, C. L. J., Martin, P., and Sanders, R. J.: Where is mineral ballast important for surface export of particulate organic carbon in the ocean?, Geophysical Research Letters, doi: 10.1002/2014GL061678, 2014. 2014GL061678, 2014.

Le Moigne, F. A. C., Sanders, R. J., Villa-Alfageme, M., Martin, A. P., Pabortsava, K., Planquette, H., Morris, P. J., and Thomalla, S. J.: On the proportion of ballast versus non-ballast associated carbon export in the surface ocean, Geophys. Res. Lett., 39, L15610, 2012.

Lima, I. D., Lam, P. J., and Doney, S. C.: Dynamics of particulate organic carbon flux in a global ocean model, Biogeosciences Discuss., 10, 14715-14767, 2013.

Lomas, M. W., Steinberg, D. K., Dickey, T., Carlson, C. A., Nelson, N. B., Condon, R. H., and Bates, N. R.: Increased ocean carbon export in the Sargasso Sea linked to climate variability is countered by its enhanced mesopelagic attenuation, Biogeosciences, 7, 57-70, 2010.

Maiti, K., Benitez-Nelson, C. R., Rii, Y., and Bidigare, R.: The influence of a mature cyclonic eddy on particle export in the lee of Hawaii, Deep Sea Research Part II: Topical Studies in Oceanography, 55, 1445-1560, 2012.

Martin, J. H., Knauer, G. A., Karl, D. M., and Broenkow, W. W.: Vertex - Carbon Cycling in the Northeast Pacific, Deep-Sea Research Part a-Oceanographic Research Papers, 34, 267-285, 1987.

Martin, P., Lampitt, R. S., Jane Perry, M., Sanders, R., Lee, C., and D'Asaro, E.: Export and mesopelagic particle flux during a North Atlantic spring diatom bloom, Deep Sea Research Part I: Oceanographic Research Papers, 58, 338-349, 2011.

McCave, I. N.: Vertical flux of particles in the ocean, Deep Sea Research, 22, 491-502, 1975.

McDonnell, A. M. P. and Buesseler, K. O.: Variability in the average sinking velocities of marine particles, Limnology and Oceanography, 55, 2085-2096, 2010.

Michaels, A. F. and Silver, M. W.: Primary production, sinking fluxes and the microbial food web, Deep Sea Research Part A. Oceanographic Research Papers, 35, 473-490, 1988.

Morris, P. J., Sanders, R., Turnewitsch, R., and Thomalla, S.: Th-234-derived particulate organic carbon export from an island-induced phytoplankton bloom in the Southern Ocean, Deep-Sea Research Part Ii-Topical Studies in Oceanography, 54, 2208-2232, 2007.

Owens, S., Buesseler, K., and Sims, K.: Re-evaluating the ^{238}U-salinity relationship in seawater: Implications for the ^{238}U–^{234}Th disequilibrium method, Marine Chemistry, 127, 31-39, 2011.

Paasche, E. and Brubak, S.: Enhanced calcification in the coccolithophorid *Emiliania huxleyi* (Haptophyceae) under phosphorus limitation, Phycologia, 33, 324-330, 1994.

Passow, U. and De la Rocha, C. L.: Accumulation of mineral ballast on organic aggregates, Global Biogeochemical Cycles, 20, 2006.

Pike, S. M., Buesseler, K. O., Andrews, J., and Savoye, N.: Quantification of Th-234 recovery in small volume sea water samples by inductively coupled plasma-mass spectrometry, Journal of Radioanalytical and Nuclear Chemistry, 263, 355-360, 2005.

Pilson, M. E. Q.: An Introduction to the Chemistry of the Sea, Cambridge University Press, New York, 2012. 2012.

Planchon, F., Cavagna, A.-J., Cardinal, D., André, L., and Dehairs, F.: Late summer particulate organic carbon export and twilight zone remineralisation in the Atlantic sector of the Southern Ocean, Biogeosciences, 10, 803-820, 2013.

Resplandy, L., Martin, A. P., Le Moigne, F., Martin, P., Aquilina, A., Mémery, L., Lévy, M., and Sanders, R.: How does dynamical spatial variability impact ^{234}Th-derived estimates of organic export?, Deep Sea Research Part I: Oceanographic Research Papers, 68, 24-45, 2012.

Riley, J. S., Sanders, R., Marsay, C., Le Moigne, F. A. C., Achterberg, E. P., and Poulton, A. J.: The relative contribution of fast and slow sinking particles to ocean carbon export, Global Biogeochem. Cycles, 26, GB1026, 2012.

Rodriguez y Baena, A. M., Boudjenoun, R., Fowler, S. W., Miquel, J. C., Masqué, P., Sanchez-Cabeza, J.-A., and Warnau, M.: ^{234}Th-based carbon export during an ice-edge bloom: Sea-ice algae as a likely bias in data interpretation, Earth and Planetary Science Letters, 269, 596-604, 2008.

Rosenheim, B. E., Day, M. B., Domack, E., Schrum, H., Benthien, A., and Hayes, J. M.: Antarctic sediment chronology by programmed-temperature pyrolysis: Methodology and data treatment, Geochemistry, Geophysics, Geosystems, 9, 2008.

Rosenheim, B. E. and Galy, V.: Direct measurement of riverine particulate organic carbon age structure, Geophysical Research Letters, 39, 2012.

Rosenheim, B. E., Roe, K. M., Roberts, B. J., Kolker, A. S., Allison, M. A., and

Johannesson, K. H.: River discharge influences on particulate organic carbon age structure in the Mississippi/Atchafalaya River System, Global Biogeochemical Cycles, 27, 154-166, 2013.

Rutgers van der Loeff, M. M., Cai, P. H., Stimac, I., Bracher, A., Middag, R., Klunder, M. B., and van Heuven, S. M.: ^{234}Th in surface waters: Distribution of particle export flux across the Antarctic Circumpolar Current and in the Weddell Sea during the GEOTRACES expedition ZERO and DRAKE, Deep Sea Research Part II: Topical Studies in Oceanography, 58, 2749-2766, 2011.

Rutgers Van Der Loeff, M. M., Friedrich, J., and Bathmann, U. V.: Carbon export during the Spring Bloom at the Antarctic Polar Front, determined with the natural tracer ^{234}Th, Deep Sea Research Part II: Topical Studies in Oceanography, 44, 457-478, 1997.

Rutgers van der Loeff, M. M., Sarin, M. M., Baskaran, M., Benitez-Nelson, C., Buesseler, K. O., Charette, M., Dai, M., Gustafsson, r., Masque, P., Morris, P. J., Orlandini, K., Rodriguez y Baena, A., Savoye, N., Schmidt, S., Turnewitsch, R., Vˆge, I., and Waples, J. T.: A review of present techniques and methodological advances in analyzing ^{234}Th in aquatic systems, Marine Chemistry, 100, 190-212, 2006.

Sanders, R., Morris, P. J., Poulton, A. J., Stinchcombe, M. C., Charalampopoulou, A., Lucas, M. I., and Thomalla, S. J.: Does a ballast effect occur in the surface ocean?, Geophysical Research Letters, 37, L08602, 2010.

Santschi, P., Murray, J. W., Baskaran, M., Benitez-Nelson, C. R., Guo, L., Hung, C.-C., Lamborg, C., Moran, S. B., Passow, U., and Roy-Barman, M.: Thorium speciation in seawater, Marine Chemistry, 100, 250-268, 2006.

Sarmiento, J. L., Dunne, J., Gnanadesikan, A., Key, R. M., Matsumoto, K., and Slater,

R.: A new estimate of the $CaCO_3$ to organic carbon export ratio, Global Biogeochemical Cycles, 16, 2002.

Sarmiento, J. L., Gruber, N., Brzezinski, M. A., and Dunne, J. P.: High-latitude controls of thermocline nutrients and low latitude biological productivity, Nature, 427, 56-60, 2004.

Savoye, N., Benitez-Nelson, C., Burd, A. B., Cochran, J. K., Charette, M., Buesseler, K. O., Jackson, G. A., Roy-Barman, M., Schmidt, S., and Elskens, M.: Th-234 sorption and export models in the water column: A review, Marine Chemistry, 100, 234-249, 2006.

Savoye, N., Trull, T. W., Jacquet, S. H. M., Navez, J., and Dehairs, F.: ^{234}Th-based export fluxes during a natural iron fertilization experiment in the Southern Ocean (KEOPS), Deep Sea Research Part II: Topical Studies in Oceanography, 55, 841-855, 2008.

Shimmield, G. B., Ritchie, G. D., and Fileman, T. W.: The Impact of Marginal Ice-Zone Processes on the Distribution of Pb-210, Po-210 and Th-234 and Implications for New Production in the Bellingshausen Sea, Antarctica, Deep-Sea Research Part Ii-Topical Studies in Oceanography, 42, 1313-1335, 1995.

Smetacek, V., Klaas, C., Strass, V. H., Assmy, P., Montresor, M., Cisewski, B., Savoye, N., Webb, A., d'Odivio, F., Arrieta, J. M., Bathmann, U., Bellerby, R., Berg, G. M., Croot, P., Gonzalez, S., Henjes, J., Herndl, G. J., Hoffmann, L. J., Leach, H., Losch, M., Mills, M. M., Neill, C., Peeken, I., Röttgers, R., Sachs, O., Sauter, E., Schmidt, M. M., Schwarz, J., Terbrüggen, A., and Wolf-Gladrow, D.: Deep carbon export from a Southern Ocean iron-fertilized diatom bloom, Nature, 487, 7407, 313-319, 2012.

Sokolov, S. and Rintoul, S. R.: Circumpolar structure and distribution of the Antarctic

Circumpolar Current fronts: 1. Mean circumpolar paths, Journal of Geophysical Research: Oceans (1978–2012), 114, 2009.

Steinberg, D. K., Van Mooy, B. A. S., Buesseler, K. O., Boyd, P. W., Kobari, T., and Karl, D. M.: Bacterial vs. zooplankton control of sinking particle flux in the ocean's twilight zone, Limnology and Oceanography, 53, 1327-1338, 2008.

Strickland, J. D. and Parsons, T. R.: A practical handbook of seawater analysis, Fisheries Research Board of Canada Ottawa, 1968.

Thomalla, S., Turnewitsch, R., Lucas, M., and Poulton, A.: Particulate organic carbon export from the North and South Atlantic gyres: The $^{234}Th/^{238}U$ disequilibrium approach, Deep Sea Research Part II: Topical Studies in Oceanography, 53, 1629-1648, 2006.

Thomalla, S. J., Poulton, A. J., Sanders, R., Turnewitsch, R., Holligan, P. M., and Lucas, M. I.: Variable export fluxes and efficiencies for calcite, opal, and organic carbon in the Atlantic Ocean: A ballast effect in action?, Global Biogeochem. Cycles, 22, GB1010, 2008.

Trull, T. W., Bray, S. G., Buesseler, K. O., Lamborg, C. H., Manganini, S., Moy, C., and Valdes, J.: In situ measurement of mesopelagic particle sinking rates and the control of carbon transfer to the ocean interior during the Vertical Flux in the Global Ocean (VERTIGO) voyages in the North Pacific, Deep-Sea Research Part Ii-Topical Studies in Oceanography, 55, 1684-1695, 2008.

Volk, T. and Hoffert, M. I.: Ocean carbon pumps: Analysis of relative strengths and efficiencies in ocean-driven atmospheric CO_2 changes, Geophysical Monographs, 32, 99-110, 1985.

Wakeham, S. G., Peterson, M. L., Hedges, J. I., and Lee, C.: Lipid biomarker fluxes in

the Arabian Sea, with a comparison to the equatorial Pacific Ocean, Deep-Sea Research Part Ii-Topical Studies in Oceanography, 49, 2265-2301, 2002.

Wilson, J. D., Barker, S., and Ridgwell, A.: Assessment of the spatial variability in particulate organic matter and mineral sinking fluxes in the ocean interior: Implications for the ballast hypothesis, Global Biogeochemical Cycles, 26, GB4011, 2012.

Wilson, S. E., Steinberg, D. K., and Buesseler, K. O.: Changes in fecal pellet characteristics with depth as indicators of zooplankton repackaging of particles in the mesopelagic zone of the subtropical and subarctic North Pacific Ocean, Deep-Sea Research Part Ii-Topical Studies in Oceanography, 55, 1636-1647, 2008.

Zhou, K., Nodder, S., Dai, M., and Hall, J.: Insignificant enhancement of export flux in the highly productive subtropical front, east of New Zealand: a high resolution study of particle export fluxes based on ^{234}Th: ^{238}U disequilibria, Biogeosciences, 9, 973-992, 2012.

Table 1. Locations and times of sampling of total ^{234}Th and size-fractionated particles on cruises GB1 and GB2. Two export depths are indicated: z_{PAR} (depth of 0.3% of surface photosynthetically available radiation) and $z_{Th/U}$ (depth where ^{234}Th and ^{238}U activities return to secular equilibrium below surface deficits).

Cruise	**Station**	**Date**	**Lat.**	**Long.**	**z_{PAR}**	**$z_{Th/U}$**
-	-	*dd-mm-yy*	*deg. N*	*deg. E*	*m*	*m*
GB1	6	14 Jan 2011	-51.79	-56.11	79	130
GB1	16	17 Jan 2011	-46.26	-59.83	62	141
GB1	25	20 Jan 2011	-45.67	-48.95	62	115
GB1	32	22 Jan 2011	-40.95	-46.00	69	171
GB1	38	24 Jan 2011	-36.52	-43.38	121	121
GB1	46	26 Jan 2011	-42.21	-41.21	63	100
GB1	59	29 Jan 2011	-51.36	-37.85	60	95
GB1	70	1 Feb 2011	-59.25	-33.15	100	100
GB1	77	3 Feb 2011	-57.28	-25.98	98	100
GB1	85	5 Feb 2011	-53.65	-17.75	73	140
GB1	92	7 Feb 2011	-50.40	-10.80	59	100
GB1	101	9 Feb 2011	-46.31	-3.21	81	140
GB1	109	11 Feb 2011	-42.63	3.34	76	130
GB1	117	13 Feb 2011	-38.97	9.49	62	110
GB2	5	21 Feb 2012	-36.94	39.60	78	90
GB2	27	26 Feb 2012	-45.82	51.05	105	105
GB2	36	28 Feb 2012	-46.84	58.25	90	90
GB2	43	1 Mar 2012	-47.53	64.01	108	125
GB2	53	3 Mar 2012	-49.30	71.32	81	100
GB2	63	5 Mar 2012	-54.40	74.54	109	130
GB2	73	7 Mar 2012	-59.71	77.73	93	75
GB2	87	10 Mar 2012	-54.23	88.22	107	100
GB2	93	11 Mar 2012	-49.81	94.13	113	130
GB2	100	14 Mar 2012	-44.62	100.50	113	90
GB2	106	16 Mar 2012	-40.10	105.34	102	95
GB2	112	17 Mar 2012	-40.26	109.63	76	105
GB2	119	20 Mar 2012	-42.08	113.40	92	90

Table 2. POC fluxes, concentrations, and attenuation of >51 μm [POC] in the mesopelagic zone. Attenuation coefficient is the exponent from significant power law fits to >51 μm [POC]. z_{PAR}+100m is 100 m below z_{PAR}, as defined in the Table 1 caption. Transfer efficiency is POC flux at z_{PAR}+100m divided by POC flux at z_{PAR}. Deep >51 μm [POC] was measured at 1000 m and 800 m for GB1 and GB2, respectively. POC flux errors are propagated from ^{234}Th flux, and POC:^{234}Th errors.

Cruise	Station	Depth	>51 μm [POC] Attenuation Coefficient	^{234}Th Flux at z_{PAR} + 100m	POC:Th at z_{PAR} + 100m	POC Flux at z_{PAR} + 100m	Transfer Efficiency	>51 μm [POC] (≥800m)
-	-	*m*	*unitless*	*dpm $m^{-2}d^{-1}$*	*μmol dpm^{-1}*	*mmol $m^{-2}d^{-1}$*	*unitless*	*μM*
GB1	6	179	0.8	3,319± 128[c]	1.7	5.7 ± 0.31	1.00	0.030
GB1	16	162	1.1	2,567 ± 116[c]	2.4	6.1 ± 0.30	1.04	No data
GB1	25	162	0.4	1,074 ± 125	2.5	2.7 ± 0.37	1.76	0.013
GB1	32	169	0.9	1,581 ± 186	1.3	2.0 ± 0.25	0.86	0.006
GB1	38	221	No fit	911 ± 206	1.6	1.5 ± 0.35	0.70	0.026
GB1	46	163	1.0	1,937 ± 146	1.6	3.1 ± 0.27	0.4	0.009
GB1	59	160	0.6	2,582 ± 126[c]	3.7	9.5 ± 0.56	1.29	0.014
GB1	70	200	0.6	1,414 ± 248	3.5	5.0 ± 0.90	0.90	0.024
GB1	77	198	0.5	1,903 ± 162	2.1	4.0 ± 0.41	0.44	0.012
GB1	85	173	1.7[a]	2,076 ± 207	3.9	8.1 ± 0.83	0.41	0.035
GB1	92	159	1.1	1,339 ± 170	3.7	4.9 ± 0.64	0.61	0.019
GB1	101	181	0.8	1,774 ± 135	1.7	3.0 ± 0.24	0.83	0.019
GB1	109	176	1.0	1,719 ± 97	1.1	1.9 ± 0.13	0.87	0.006
GB1	117	162	1.1	1,258 ± 86	1.2	1.5 ± 0.13	0.87	0.005
GB2	5	178	0.5	1,402 ± 3,706[c]	1.1	1.5 ± 6.1	0.5	No data
GB2	27	205	No fit	2,063 ± 205	1.2	2.5 ± 0.30	0.71	No data
GB2	36	190	1.5	1,077 ± 194	0.9	0.93 ± 0.18	0.48	0.011
GB2	43	208	1.9	1,247 ± 200	2.2	2.7 ± 0.45	0.54	0.005
GB2	53	181	No fit	1,013 ± 220	2.0	2.0 ± 0.45	0.49	No data
GB2	63	209	1.8	1,292 ± 262	1.7	2.1 ± 0.46	0.31	0.014
GB2	73	193	1.5	807 ± 189	1.9	1.6 ± 0.37	0.48	0.008
GB2	87	207	0.7	1,213 ± 196	1.6	1.9 ± 0.34	0.60	0.013
GB2	93	213	*2.3*[b]	469 ± 249	1.6	0.77 ± 0.42	0.53	0.001
GB2	100	213	0.8	1,132 ± 190	0.7	0.80 ± 0.15	0.52	0.014
GB2	106	202	0.9	1,405 ± 186	1.3	1.8 ± 0.26	1.63	0.017
GB2	112	176	1.3	270 ± 186	0.9	0.23 ± 0.21	0.24	0.007
GB2	119	192	No fit	756 ± 218	0.8	0.57 ± 0.17	0.20	0.013

[a] attenuation coefficient is 2.35 when only fitting > 51 μm [POC] measurements at depths <500 m (Fig. 3).
[b] outlier approximated by Chauvenet's Theorem (Glover, et al., 2011).

[c]values were estimated by linear interpolation of values at upper and lower depths around z_{PAR}+100m.
"no data": no measurements at these depths.
"no fit": power-law fit was not statistically significant ($p>0.05$).

Table 3. POC, biomineral, and ^{234}Th concentrations and fluxes at z_{PAR}. Ez- ratio is ^{234}Th-derived POC flux at z_{PAR} divided by integrated primary productivity. The % >51μm [POC] metric is the fraction of total [POC] in the >51 μm size fraction. POC and biomineral flux errors are propagated from ^{234}Th flux, and POC:^{234}Th errors.

Cruise	**Station**	**z_{PAR}**	**^{234}Th Flux**	**>51um [POC]**	**>51um [Bsi]**	**>51um [PIC]**	**>51um Th activity**	**POC:Th**	**POC Flux**	**Bsi:Th**	**BSi Flux**	**PIC:Th**	**PIC Flux**	**Primary Productivity**	**Ez- Ratio**	**% >51 um [POC]**
-	-	*m*	*dpm $m^{-2}d^{-1}$*	*uM*	*uM*	*uM*	*dpm L^{-1}*	*μmol dpm^{-1}*	*mmol $m^{-2}d^{-1}$*	*μmol dpm^{-1}*	*mmol $m^{-2}d^{-1}$*	*μmol dpm^{-1}*	*mmol $m^{-2}d^{-1}$*	*mmol $m^{-2}d^{-1}$*	*unitless*	*%*
GB1		6	79	2,437 ± 100	0.23 [b]	0.03[a]	0.124 [a]	0.07 [a]	2.3 [a]	5.7 ± 0.26	0.4	0.9 ± 0.04	1.8	4.3 ± 0.20	42	0.14	8.8%
GB1		16	62	1,933 ± 71	0.38	0.08	0.390	0.12	3.0	5.9 ± 0.68	0.6	1.2 ± 0.14	3.1	6.1 ± 0.70	165	0.04	17.7%
GB1		25	62	862 ± 46 [a]	0.04	0.005 [a]	0.015 [a]	0.02	1.8	1.6 ± 0.11	0.2	0.2 ± 0.02	0.7	0.6 ± 0.04	35	0.04	3.2%
GB1		32	69	1,304 ± 116	0.07	0.01	0.027	0.04	1.8	2.3 ± 0.21	0.3	0.3 ± 0.03	0.7	0.9 ± 0.08	11	0.21	3.9%
GB1		38	121	809 ± 126	0.04	0.003	0.017	0.01	2.7	2.2 ± 0.35	0.2	0.2 ± 0.03	1.2	0.9 ± 0.15	21	0.10	8.4%
GB1		46	63	2,123 ± 69	0.23	0.005	0.059	0.06	4.1	8.8 ± 0.38	0.1	0.2 ± 0.02	1.1	2.2 ± 0.10	13	0.67	5.3%
GB1		59	60	1,844 ± 102	0.09	0.10	0.072	0.02	4.0	7.3 ± 0.52	4.6	8.6 ± 0.53	3.4	6.2 ± 0.39	26	0.28	5.3%
GB1		70	100	1,280 ± 94	0.11	0.06[a]	0.001 [a]	0.02	4.3	5.5 ±	3.5 [a]	4.5 ±	0.1 [a]	0.1 ±	10	0.53	10.6%

									0.44		0.35		0.09			
GB1	77	98	1,485 ± 105	0.03	0.03	0.002	0.01	6.0	9.0 ± 1.3	5.6	8.3 ± 0.98	0.4	0.7 ± 0.23	57	0.16	3.6%
GB1	85	73	1,858 ± 94	2.50	3.44	0.124	0.23	10.8	20 ± 1.1	14.9	28 ± 1.5	0.5	1.0 ± 0.05	53	0.38	52.0%
GB1	92	59	1,639 ± 77	0.40	0.46	0.020	0.08	4.9	8.0 ± 0.40	5.6	9.3 ± 0.46	0.2	0.4 ± 0.02	26	0.31	11.3%
GB1	101	81	1,763 ± 82	0.19	0.05	0.013	0.09	2.0	3.6 ± 0.18	0.5	0.9 ± 0.04	0.1	0.2 ± 0.01	22	0.17	12.5%
GB1	109	76	1,524 ± 76	0.19 [a]	0.05 [a]	0.027 [a]	0.14 [a]	1.4	2.1 ± 0.11	0.4	0.6 ± 0.03	0.2	0.3 ± 0.02	14	0.16	21.0%
GB1	117	62	1,177 ± 50	0.21	0.02	0.032	0.15	1.4	1.7 ± 0.07	0.1	0.2 ± 0.01	0.2	0.3 ± 0.01	18	0.09	6.6%
GB2	5	78	1,889 ± 5207	0.08 [b]	0.01 [a]	0.048 [a]	0.05 [a]	1.6	3.0 ± 8.8	0.2	0.4 ± 1.2	1.0	1.9 ± 5.2	8.2	0.37	7.6%
GB2	27	105	1,869 ± 160	0.08 [a]	0.10 [a]	0.060 [a]	0.04 [a]	1.9	3.5 ± 0.32	2.2	4.0 ± 0.35	1.3	2.5 ± 0.22	8.0	0.44	6.7%
GB2	36	90	988 ± 89	0.43	0.28	0.074	0.22	2.0	2.0 ± 0.18	1.3	1.3 ± 0.12	0.3	0.3 ± 0.03	12	0.16	15.6%
GB2	43	108	1,221 ± 153	0.74 [a]	0.62 [a]	0.041 [a]	0.18 [a]	4.1	5.0 ± 0.63	3.4	4.2 ± 0.53	0.2	0.3 ± 0.04	12	0.43	37.8%
GB2	53	81	1058 ± 100 [a]	0.54 [a]	0.80 [a]	0.081 [a]	0.14 [a]	3.9	4.1 ± 0.40	5.7	6.1 ± 0.59	0.6	0.6 ± 0.07	16	0.25	22.5%
GB2	63	109	1,229 ± 138	0.71 [a]	1.04 [a]	0.028 [a]	0.13 [a]	5.6 [a]	6.9 ± 0.78	8.1	9.9 ± 1.1	0.2	0.3 ± 0.03	9.0	0.77	33.2%
GB2	73	93	977 ± 108	0.21 [b]	1.13 [a]	0.014 [a]	0.20 [a]	3.3 [a]	3.2 ± 0.36	5.6	5.4 ± 0.60	0.1	0.1 ± 0.01	8.8	0.36	17.6%

GB2	87	107	1,299 ± 115	0.06 [b]	0.30 [a]	0.041 [a]	0.06 [a]	2.5 [a]	3.2 ± 0.40	4.7	6.1 ± 0.55	0.6	0.8 ± 0.14	11	0.29	3.4%
GB2	93	113	1,142 ± 137	0.07 [a]	0.01 [a]	0.023 [a]	0.05 [a]	1.3	1.5 ± 0.25	0.2	0.3 ± 0.06	0.4	0.5 ± 0.14	12	0.12	4.3%
GB2	100	113	1,112 ± 130	0.08	0.02	0.006	0.06	1.4	1.5 ± 0.19	0.3	0.3 ± 0.04	0.1	0.1 ± 0.02	14	0.11	12.8%
GB2	106	102	1394 ± 82 [a]	0.09 [b]	0.04 [a]	0.024 [a]	0.12 [a]	0.8	1.1 ± 0.86	0.3 [a]	0.4 ± 0.02	0.2	0.3 ± 0.02	22	0.05	12.2%
GB2	112	76	717 ± 97	0.22 [b]	0.17 [a]	0.087 [a]	0.36 [a]	1.4 [a]	1.0 ± 0.13	0.5	0.3 ± 0.05	0.2	0.2 ± 0.02	no data	no data	13.3%
GB2	119	92	1,223 ± 124	0.51 [a]	0.12 [a]	0.048 [a]	0.22 [a]	2.3	2.8 ± 0.29	0.5	0.7 ± 0.07	0.2	0.3 ± 0.03	17	0.17	21.5%

[a] values at z_{PAR} estimated by linear interpolation of values at upper and lower depths around z_{PAR}.
[b] >51 µm [POC] values interpolated by significant power-law fits (Fig. 3).
"no data": not enough depths were sampled and analyzed to interpolate at z_{PAR}.

1229 Table 4. Mean ± standard deviations of ^{234}Th fluxes, POC:^{234}Th, BSi: ^{234}Th, PIC: ^{234}Th, POC fluxes, and biomineral fluxes at z_{PAR},
1230 divided by three latitude zones. 45 °S marks the approximate latitude of the Subantarctic front, while 52 °S marks the approximate
1231 latitude of the Polar front (Belkin and Gordon, 1996; Sokolov and Rintoul, 2009).
1232

Lat. zone	**^{234}Th Flux at z_{PAR}**	**POC:Th at z_{PAR}**	**POC Flux at z_{PAR}**	**BSi:Th at z_{PAR}**	**BSi Flux at z_{PAR}**	**PIC:Th at z_{PAR}**	**PIC Flux at z_{PAR}**	**# stn**
°S	*dpm $m^{-2}d^{-1}$*	*µmol dpm^{-1}*	*mmol $m^{-2}d^{-1}$*	*µmol dpm^{-1}*	*mmol $m^{-2}d^{-1}$*	*µmol dpm^{-1}*	*mmol $m^{-2}d^{-1}$*	-
36 - 45	1.3 ± 0.44	1.9 ± 0.9	2.7 ± 2.3	0.3 ± 0.1	0.33 ± 0.17	0.5 ± 0.4	0.73 ± 0.76	10
45 – 52	1.5 ± 0.50	2.8 ±1.2	4.4 ± 2.2	2.3 ± 2.2	3.4 ± 3.3	1.1 ± 1.2	2.0 ± 2.4	11
52 - >60	1.4 ± 0.30	5.4 ± 3.0	8.0 ± 6.3	7.1 ± 4.1	10 ± 8.7	0.3 ± 0.2	0.49 ± 0.4	6

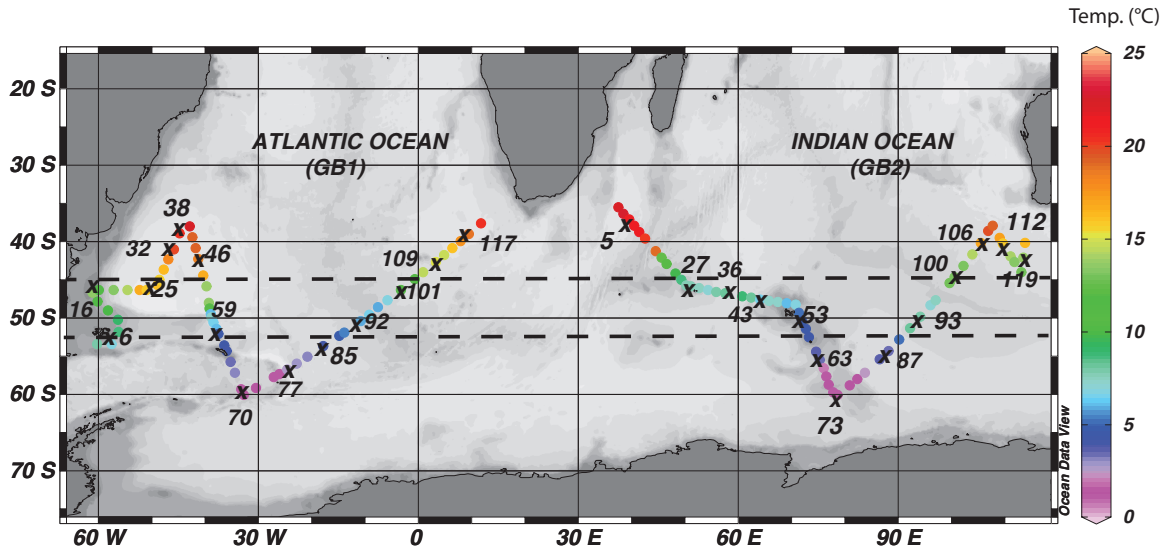

Figure 1. Cruise tracks across the Atlantic (cruise GB1) and Indian (cruise GB2) sectors of the Great Calcite Belt showing sea surface temperature along the two transects. Station numbers where only ^{234}Th and size-fractionated particles were sampled are indicated by crosses. The two horizontal dashed lines at 45 °S and 52 °S represent the approximate locations of the Subantarctic and Polar fronts, respectively (Belkin and Gordon, 1996; Sokolov and Rintoul, 2009).

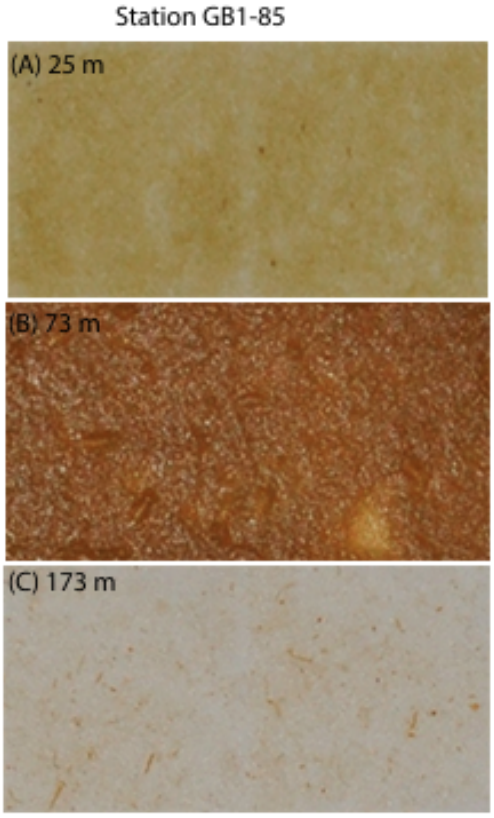

Figure 2. Digital images of >51 µm filters from station GB1-85 (refer to Fig. 1 for station location). >51 µm particles are from (a) 25m in the euphotic zone, (b) 73m, which corresponds to z_{PAR}, as defined in Table 1, and (c) at 173m, below both metrics of export depth, z_{PAR} and $z_{Th/U}$ (Table 1). >51 µm particles in the euphotic zone appear as dense sheets of intact cells packed onto the filters (a, b) and as more sparsely arranged cylindrical fecal pellets on filters collected below z_{PAR} (c).

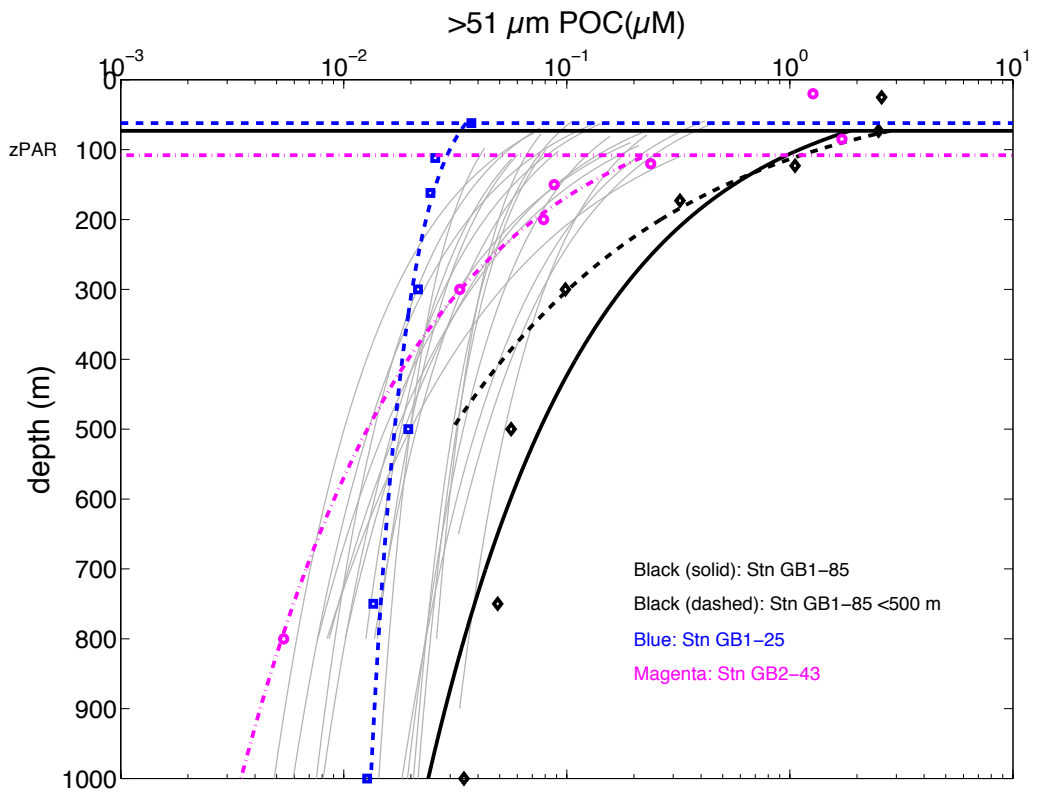

1251

1252 Figure 3. Significant power law fits of >51 μm [POC] below z_{PAR}, according to Eq. (1).
1253 Only the 22 significant fits are shown as lines. Three stations are highlighted to show the
1254 range in >51 μm [POC] attenuation across GB1 and GB2 profiles (symbols represent
1255 measurements): GB1-85 had the highest POC concentration through the water column
1256 and an attenuation coefficient of 1.7; GB1-25 had the lowest attenuation coefficient (0.4);
1257 GB2-43 had the highest attenuation coefficient (1.9) (Table 2). Fitting GB1-85 >51 μm
1258 [POC] measurements between z_{PAR} and 500 m yields a higher attenuation coefficient of
1259 2.35. Refer to Fig. 1 for station locations.

1260

1261

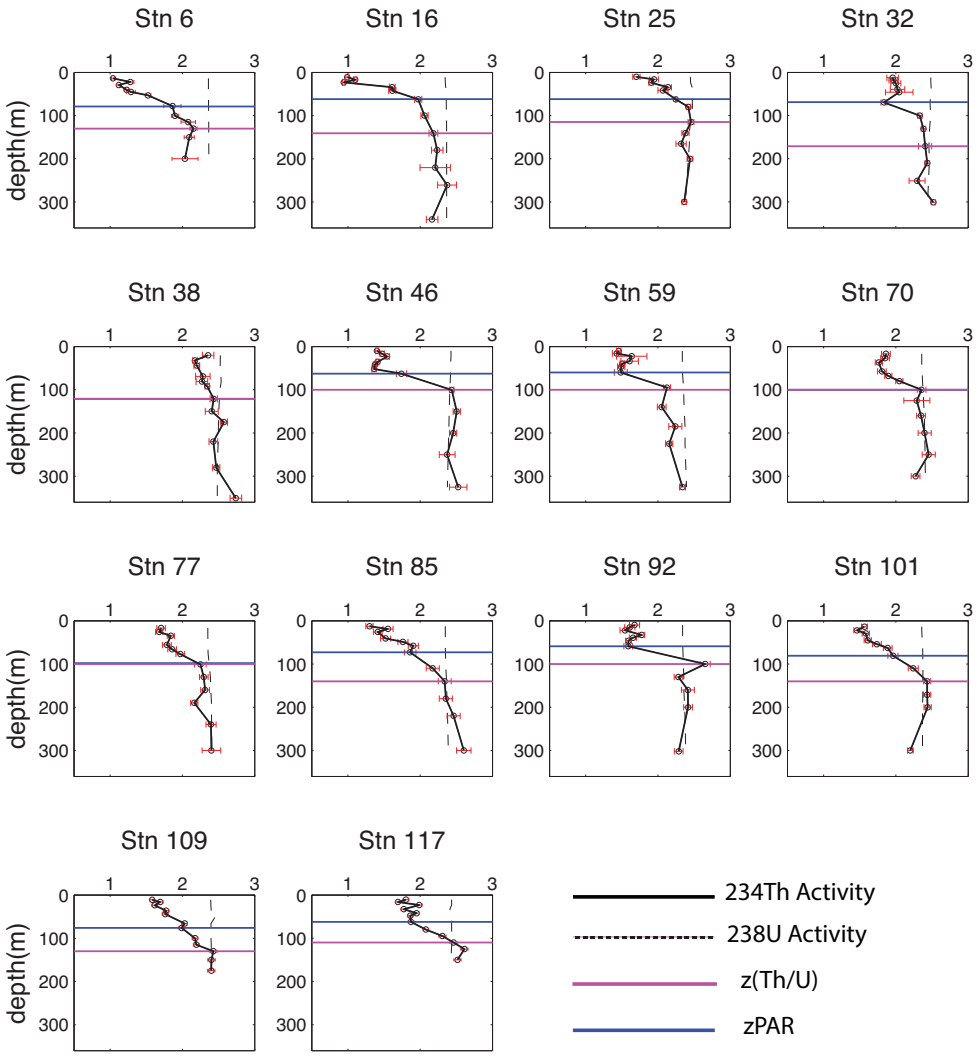
Stn 6
Stn 16
Stn 25
Stn 32
Stn 38
Stn 46
Stn 59
Stn 70
Stn 77
Stn 85
Stn 92
Stn 101
Stn 109
Stn 117
depth(m)
0
100
200
300
1
2
3
234Th Activity
238U Activity
z(Th/U)
zPAR

1262

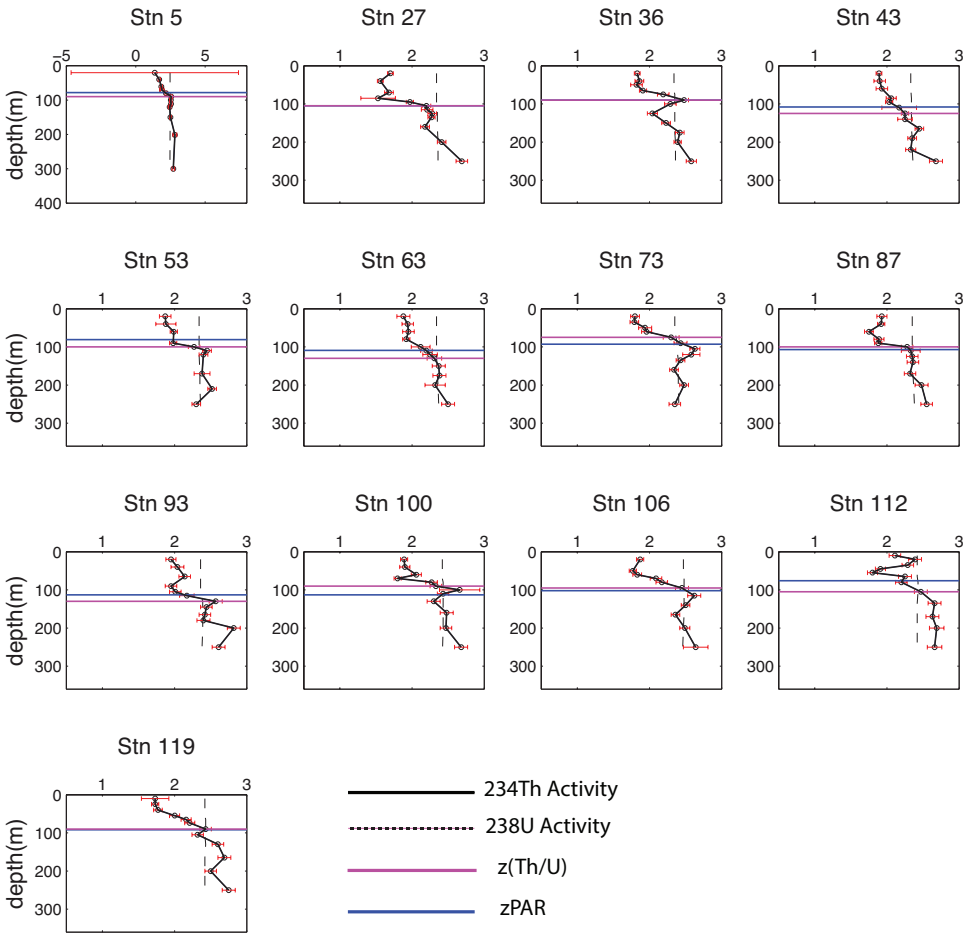

Figure 4. Total ^{234}Th and ^{238}U activity profiles measured at 14 stations of GB1 and 13 stations of GB2 (note different x-axis for station GB2-5) (Table S1). Error bars for ^{234}Th activity are propagated errors. ^{238}U is calculated from salinity. All ^{234}Th activity profiles exhibit a deficit relative to ^{238}U activity at the surface, and mostly return to equilibrium with ^{234}U within error at depth of $z_{Th/U}$ (Table 1). Refer to Fig. 1 for station locations.

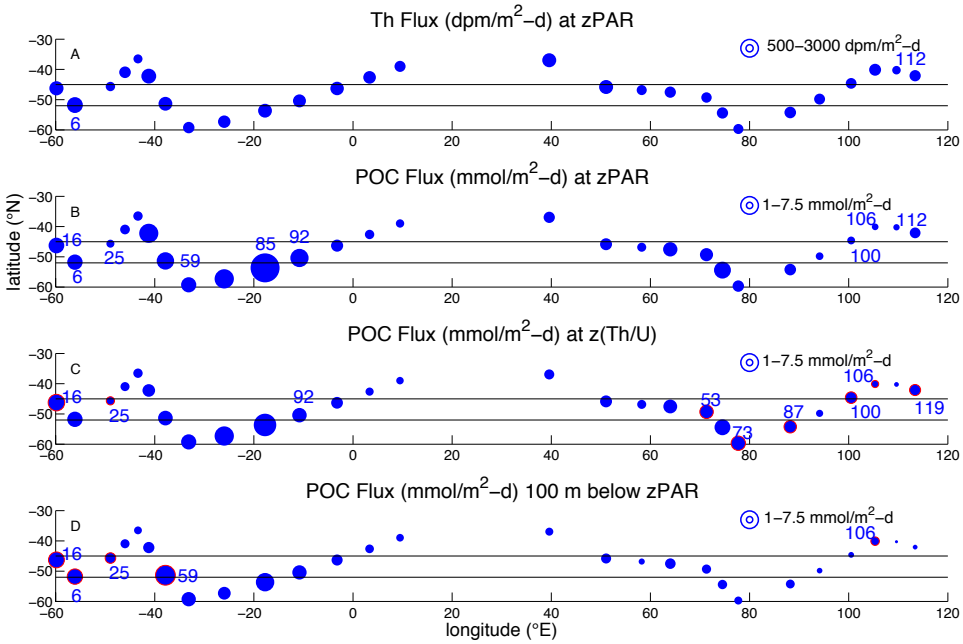

Figure 5. Distribution of ^{234}Th flux and ^{234}Th-derived POC flux at 27 stations along GB1 and GB2 (circle area scales with flux magnitude). (a) ^{234}Th fluxes at z_{PAR} range from 717 dpm m^{-2} d^{-1} to 2,437 dpm m^{-2} d^{-1} at stations GB2-112 and GB1-6, respectively. (b) POC fluxes at z_{PAR} range from 0.97 mmol m^{-2} d^{-1} to 20 mmol m^{-2} d^{-1}at stations GB2-112 and GB1-85, respectively. (c) POC fluxes at $z_{Th/U}$ range from 0.57 to 12 mmol m^{-2} d^{-1} at stations GB2-112 and GB1-85, respectively (Table S2). (d) POC fluxes at 100m below z_{PAR} range from 0.23 to 9.5 mmol m^{-2} d^{-1} at stations GB2-112 and GB1-59, respectively. A few station numbers discussed in the text are indicated. Red outlines distinguish stations where fluxes are greater at the specified depth than at z_{PAR}. The two horizontal dashed lines at 45 °S and 52 °S represent the approximate locations of the Subantarctic and Polar fronts, respectively (Belkin and Gordon, 1996; Sokolov and Rintoul, 2009). Refer to Fig. 1 for other station locations. z_{PAR} and $z_{Th/U}$ are defined as in Table 1.

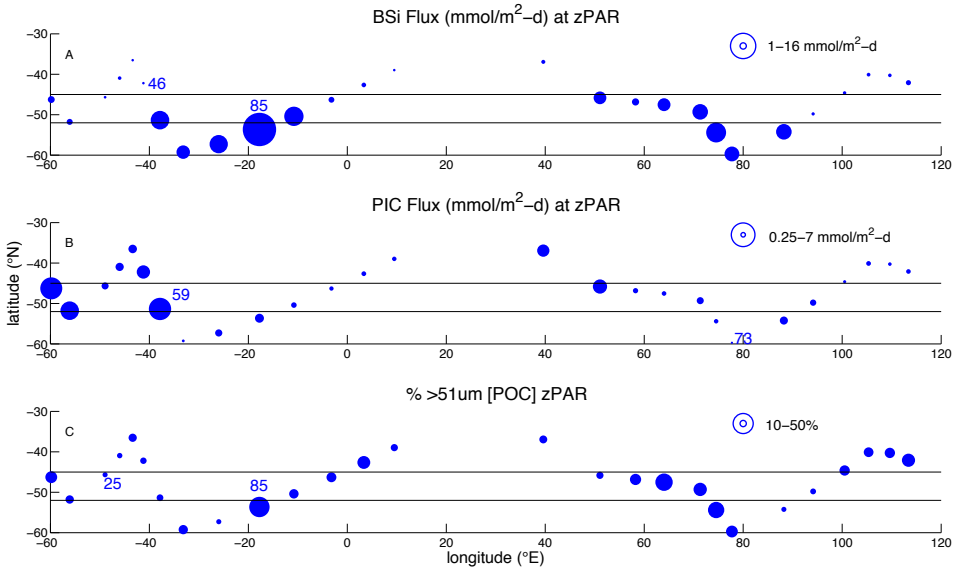

1286

1287 Figure 6. Distribution of BSi flux, PIC flux, and % >51 µm [POC], the percent of total
1288 [POC] in the >51 µm size class, at z_{PAR} (Table 1) along GB1 and GB2 (circle area scales
1289 with magnitude). (a) BSi fluxes range from 0.17 mmol m^{-2} d^{-1} to 28 mmol m^{-2} d^{-1} at
1290 stations GB1-46 and GB1-85, respectively. (b) PIC fluxes range from 0.067 to 6.2 mmol
1291 m^{-2} d^{-1}at stations GB2-73 and GB2-59, respectively. (c) The proportion of [POC] in the
1292 >51 µm size-fraction at z_{PAR} ranges from 3.3% to 52% at stations GB1-25 and GB1-85,
1293 respectively. A few station numbers discussed in the text are indicated. The two
1294 horizontal dashed lines at 45 °S and 52 °S represent the approximate locations of the
1295 Subantarctic and Polar fronts, respectively (Belkin and Gordon, 1996; Sokolov and
1296 Rintoul, 2009). Refer to Fig. 1 for other station locations.

1297

1298

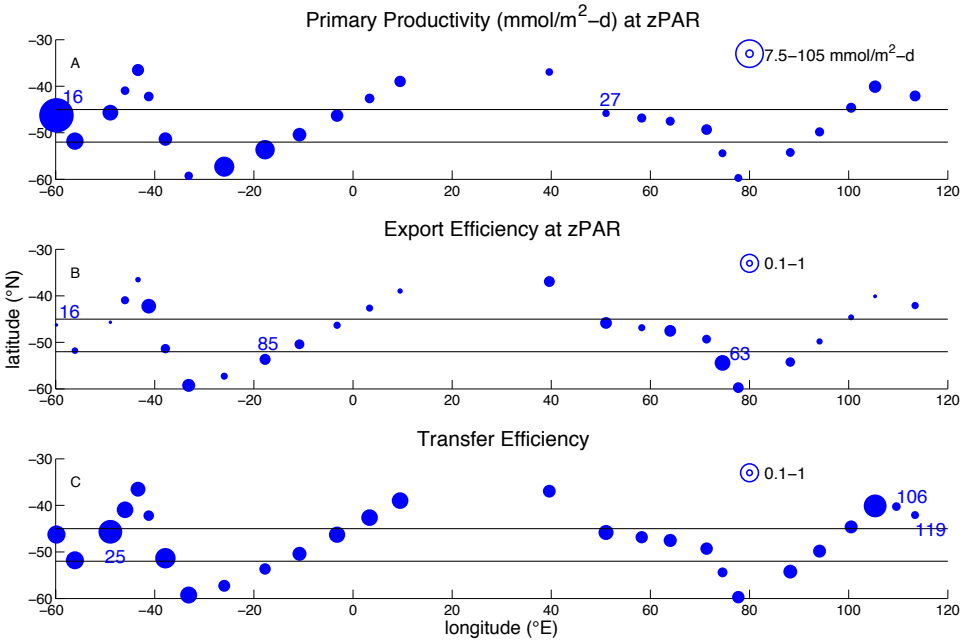

Figure 7. Distribution of primary productivity, export efficiency, and transfer efficiency along GB1 and GB2 (circle area scales with magnitude). (a) Primary productivity integrated through the euphotic zone ranges from 8.0 to 165 mmol m^{-2} d^{-1} at stations GB2-27 and GB1-16, respectively. (b) Export efficiency (Ez-ratio) at z_{PAR} (Table 1), which is the ratio of ^{234}Th-derived POC flux at z_{PAR} to primary productivity integrated to z_{PAR}, ranges from 0.04 to 0.77 at stations GB1-16 and GB2-63, respectively. (c) Transfer efficiency at z_{PAR}, which is the ratio of POC flux 100 m below z_{PAR} to POC flux at z_{PAR}, ranges from 0.20 to 1.8 at stations GB1-119 and GB1-25, respectively. A few station numbers discussed in the text are indicated. The two horizontal dashed lines at 45 °S and 52 °S represent the approximate locations of the Subantarctic and Polar fronts, respectively (Belkin and Gordon, 1996; Sokolov and Rintoul, 2009). Refer to Fig. 1 for other station locations.

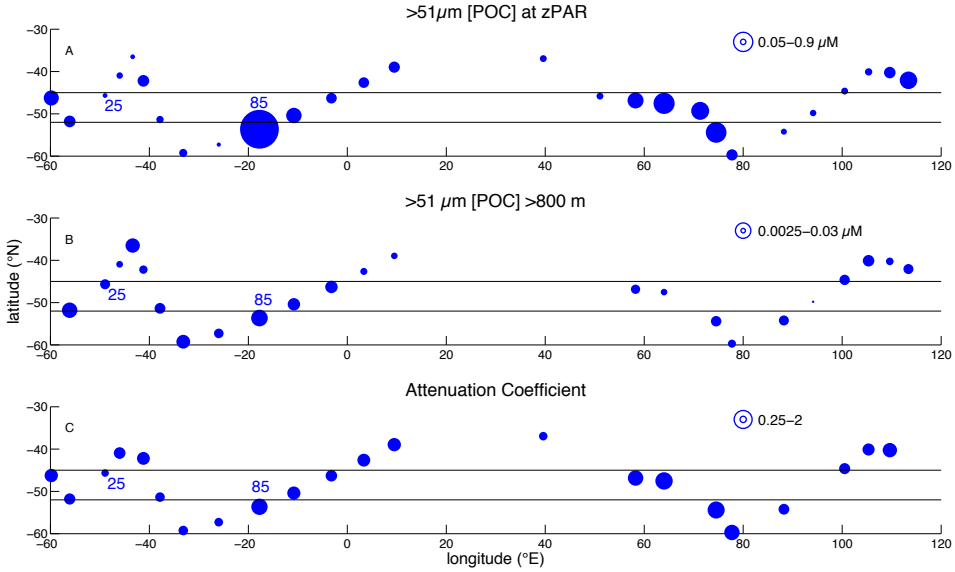

1314

1315 Figure 8. Distribution and vertical attenuation coefficient of >51 µm [POC] (circle area
1316 scales with magnitude). (a) >51 µm POC concentrations at z_{PAR} (Table 1) range from
1317 0.03 µM to 2.5 µM at stations GB1-77 and GB1-85, respectively. (b) >51 µm [POC] at
1318 the deepest pump depth in the lower mesopelagic zone (800 m-1000 m). Concentrations
1319 range from 0.001 µM to 0.035 µM at stations GB2-93 and GB1-85, respectively. (c)
1320 Attenuation coefficient from significant power-law fits of 22 >51 µm [POC] profiles,
1321 excluding GB2-93 (see Sect. 4.4). A few station numbers discussed in the text are
1322 indicated. The two horizontal dashed lines at 45 °S and 52 °S represent the approximate
1323 locations of the Subantarctic and Polar fronts, respectively (Belkin and Gordon, 1996;
1324 Sokolov and Rintoul, 2009). Refer to Fig. 1 for other station locations.

1325

1326

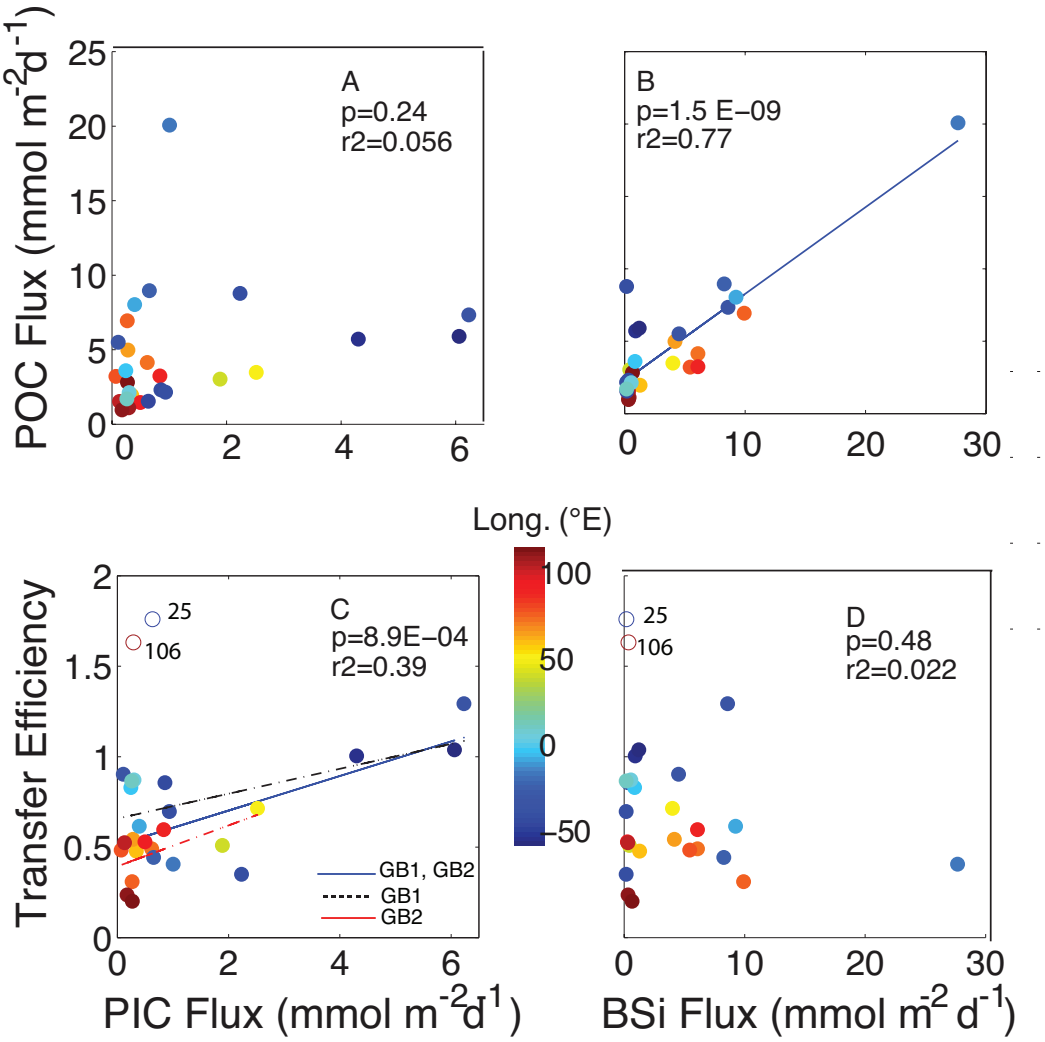

Figure 9. ^{234}Th-derived POC flux as a function of (a) PIC flux and (b) BSi flux at z_{PAR}. POC flux transfer efficiency between z_{PAR} and z_{PAR}+100 m (T_{100}, defined in Sect. 4.4) as a function of (c) PIC flux and (d) BSi flux at z_{PAR}. Significant linear relationships are plotted as a solid blue line. T_{100} values at GB1-25 and GB2-106 were excluded from all correlations (Sect. 4.4). Color bar indicates longitude of stations— GB1 and GB2 stations are in cool and warm colors, respectively. Refer to Fig. 1 for more specific station locations.

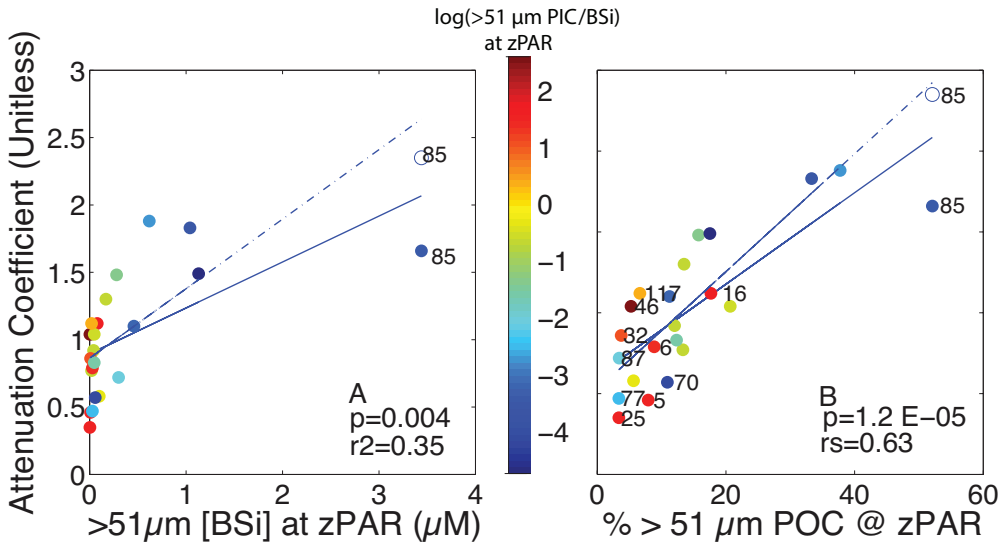

Figure 10. Attenuation coefficient as a function of (a) >51 µm [BSi] at z_{PAR} and (b) the proportion of [POC] in the >51 µm size-fraction at z_{PAR}. The open circle indicates where GB1-85 would plot with a higher attenuation coefficient of 2.35, derived from fitting >51 µm [POC] at depths between z_{PAR} and 500 m. Significant linear relationships using the lower and higher attenuation coefficient values for GB1-85 are shown as solid and dashed lines, respectively; p and r^2 values are provided for the solid lines. The color bar is the natural logarithm of the ratio of >51 µm PIC:BSi at z_{PAR}. We interpret all warm colors >0 to indicate stations with a high relative abundance of coccolithophores, and all cool values <0 to indicate stations with a high relative abundance of diatoms (Figs. S2, S3). A few station numbers discussed in the text are indicated. Refer to Fig. 1 for station locations.

1349